KfK 4411
Mai 1988

Monte Carlo Shielding Calculations in the Double Null Configuration of NET

U. Fischer
Institut für Neutronenphysik und Reaktortechnik
Projekt Kernfusion

Kernforschungszentrum Karlsruhe

Kernforschungszentrum Karlsruhe

Institut für Neutronenphysik und Reaktortechnik

Projekt Kernfusion

KfK 4411

Monte Carlo Shielding Calculations in the Double Null Configuration of NET.

U. Fischer

Kernforschungszentrum Karlsruhe GmbH, Karlsruhe

Kernforschungszentrum Karlsruhe GmbH
Postfach 3640, 7500 Karlsruhe 1

ISSN 0303-4003

Abstract

Multi - dimensional Monte Carlo shielding calculations have been performed for evaluating the shielding performance of the NET reactor components. Biased Monte Carlo techniques, that are available in the MCNP - code, have been applied for describing the neutron and photon transport through the shielding components. A realistic three - dimensional model of a NET torus sector has been used, that takes into account all relevant reactor components adequately. The poloidal variations of the physical quantities relevant for the radiation shielding, the shielding performance of the divertors, and the neutron streaming through toroidal segment gaps and its impact on the shielding performance of the vacuum vessel are the main objects of the analysis. Furthermore, the relations between idealized one - dimensional and realistic three - dimensional shielding calculations are analyzed.

Monte - Carlo - Abschirmrechnungen in der Doppel Null Konfiguration von NET.

Zusammenfassung

Zur Beurteilung des Abschirmvermögens der Reaktorkomponenten von NET wurde eine Analyse durchgeführt, die sich auf dreidimensionale Monte - Carlo - Rechnungen stützt. Hierzu wurden Varianzreduktionsmethoden angewandt, die in dem Monte - Carlo - Transportprogramm MCNP verfügbar sind. Es wurde ein realistisches dreidimensionales Modell eines NET - Torussektors zugrunde gelegt, das alle maßgeblichen Reaktorkomponenten zweckmäßig berücksichtigt. Schwerpunktmäßig befaßt sich die Analyse mit der poloidalen Abhängigkeit der für die Strahlenabschirmung maßgeblichen physikalischen Größen, dem Abschirmvermögen der Divertoren, sowie dem Neutronenstreaming in den Segmentspalten und dessen Einfluß auf das Abschirmverhalten des Vakuumgefäßes. Darüberhinaus werden die Beziehungen zwischen idealisierten eindimensionalen und realistischen dreidimensionalen Abschirmrechnungen untersucht.

Contents

1. Introduction

The design of the NET reactor provides the utilization of the blanket and the vacuum vessel as shielding components for the protection of the superconducting magnets from the neutron and photon radiation. The blanket can be utilized as breeding or as non-breeding shielding module. In both cases, however, it is used as movable shield that can be removed during reactor shut-down. In the context treated here, the blanket is regarded as shielding blanket, although actually it is a breeding blanket.

The vacuum vessel performs the function of a permant shield: it cannot be replaced during the lifetime of the NET reactor. One of its main functions is the attenuation of the neutron and photon radiation to a tolerable level. The vacuum vessel therefore has to be optimized with respect to its radiation shielding performance.

The main objective of the present work is the evaluation of the effectiveness of the NET shielding components in a three-dimensional description that is very close to reality. In the past the shielding calculations for NET have been performed in the usual one-dimensional approach, using the S_N-procedure in the torus mid-plane (e.g. /Dä 87, Bo 87, Kü 87/). The estimates gained by this simplified procedure have been sufficient in the beginning phase of the NET blanket and shield design. At present, the design phase has reached a level, where more detailed analyses have become necessary. With respect to the radiation shielding, it is necessary now to take into account the complete three-dimensional geometry in the shielding calculations. Due to the complex geometrical arrangements of blankets, divertors, shields, reflectors, plugs and openings, this task only can be accomplished by the appropriate application of the Monte Carlo method. In fact, only the biased Monte Carlo technique ("importance sampling") is suitable for this purpose.

The problems treated explicitly in this work refer to the poloidal variation of the physical quantities relevant for the radiation shielding, the shielding performance of the divertors, and the neutron streaming through gaps between neighbouring blanket segments and its impact on the shielding performance of the NET vacuum vessel. The calculations have been performed in a three-dimensional torus sector model of NET in the double null configuration. The problem of the neutron streaming through the segment gaps has been treated in a two-dimensional approach, as it is appropriate to do it in this way.

No attempt is made to optimize the vacuum vessel, the blanket or the divertors with respect to its shielding performance, since this is not the objective of the analysis, but the evaluation of the real three-dimensional geometrical effects on the radiation shielding performance. This is done with respect to the inboard section of the NET torus, equipped with the KfK ceramic breeder blanket and a water cooled steel vacuum vessel, specified by the NET team. Due to the restricted space available for the blanket and the vacuum vessel, at the inboard section the most crucial shielding problems have to be expected. If the effectiveness of the shielding components at the inboard section is sufficient, this also holds for the outboard section.

2. Calculational Procedure: The Monte Carlo Method with Importance Sampling

The total thickness of the blanket and the vacuum vessel at the inboard side of the NET torus amounts to 100 cm, providing a neutron flux attenuation of roughly 4 orders of magnitude. In other words, one of ten thousand neutrons, impinging onto the inboard first wall, succeeds in penetrating the shielding components. Consequently it is impossible to evaluate the behaviour of the penetrating radiation by applying an unbiased ("analog") Monte Carlo method.

Taking into account the complex geometrical arrangement of all relevant components in the shielding calculation, on the other hand necessitates the use of the Monte Carlo method. For treating deep penetration problems by the Monte Carlo method, appropriate variance reduction techniques have been developed over the past two decades. The basic idea of these biased Monte Carlo methods is to assign weights (or importances) to a particle. Therefore a Monte Carlo particle with a specific weight can represent one or more (or even less) physical particles; moreover, following the history of a particle, it can be split into two or more particles.

The weights of these "splitted particles" then are reduced according to their numbers; therefore, particle weight as a whole is conserved and hence the importance of a particle history on the statistical average is not altered. By increasing the number of "splitted particles" according to the physical decrease of the particle population, it is possible to keep the particle population nearly at a constant level and therefore to obtain e.g. nearly the same statistical accuracy for a given quantity at the front and the back of a thick radiation shield.

In the practical application of this importance sampling technique one of the key problems is to set up the geometrical configuration in correlation with the

choice of the particle weights in an appropriate way. The geometrical configuration has to be splitted into a sufficient number of cells and an appropriate particle weight has to be assigned to each cell. In choosing the geometrical set-up and the corresponding particle weights appropriately, the particles are biased to the spatial region of interest.

At KfK the Monte Carlo neutron and photon transport code MCNP /Bri 86/ is in use for applications in fusion neutronics. There are several variance reduction techniques available in MCNP, among which the importance sampling technique with geometry splitting is the most straightforward and most reliable one. Furthermore the importance sampling is supported in MCNP by the application of the Russian roulette game: particles that travel from regions of a higher particle weight to regions of a lower particle weight are killed with a probability corresponding to the ratio of the different particle weights. In this way computing time is saved, although the variance of a particle history is increased in general.

MCNP also possesses a special feature, that is very important in shielding calculations: it uses the basic nuclear data in the continuous energy representation as they are given on the nuclear data files. In contrast, the use of group nuclear data, as it is typical for deterministic neutron transport procedures, in principle necessitates the application of different problem- and space-dependent group constant sets within one calculation. This is partially due to the spatially strongly varying neutron spectrum throughout the blanket and the shield. Thus, for a reliable shielding calculation using group nuclear data, it would be mandatory to generate for each problem a set of group constant sets, each of which would have to be gained in an iterative process for a specific spatial region of the blanket or shield! In practice, however, usually one single group constant set is used: in general this is sufficient for most applications in fusion neutronics while it is not for shielding calculations!

In order to check the reliability of shielding calculations with MCNP a computational benchmark for the deep penetration of 14 MeV neutrons into iron slabs has been analysed /Fi 88/. In fact, the treatment of this typical shielding problem with MCNP provides the most reliable results for the neutron flux densities and the neutron spectra in the thick (up to 3 m) iron slabs. In contrast,the use of a unshielded group constant set results in a considerable underestimation of the penetrating neutron and photon radiation. Depending on the thickness of the iron slabs, the underestimation amounts to the factor 2 at 1m, and to roughly one order of magnitude at 3 m depth /Fi 88/.

It is concluded therefore, that the application of MCNP with importance sampling and geometry splitting is appropriate and reliable for the shielding analysis of the NET reactor.

3. Geometry and Modelling of a NET Torus Sector

The layout of the NET reactor provides 16 toroidal blanket sectors, each of which is composed of three blanket segments. In the hypothetic case, that all blanket sectors are equipped with the same blanket configuration, there are 48 identical blanket segments. Regarding the fusion neutronics of a specific blanket and shield design, it is therefore sufficient to treat 1/48 of the torus, i.e. a torus sector of 7.5 ° representing a real physical unity.

For the neutronics analysis of the KfK "canister blanket" with MCNP a three-dimensional torus sector model had been set up /Fi 87/. This sector model approximates the real geometrical configuration of a 7.5 ° torus sector very closely: all relevant components (blanket, shields, reflectors, divertors, plugs etc.) are taken into account adequately.This sector model also forms the basis for the present work: nothing is changed with respect to the outboard side of the sector; the same holds for the configuration of the blanket and the divertors at the inboard side. However, the reflector/shield configuration at the inboard side has been rearranged completely, as this is necessary for the shielding analyses. For the inboard vacuum vessel, acting as reflector/shield component, the NET design /Dä 87/ has been used. It consists of steel plates with water layers in between; for improving the shielding effectiveness, borated water is provided at the outside of the vessel. The radial thickness of the vacuum vessel is 65 cm, the thickness of the blanket is 35 cm at the inboard side. Therefore the total thickness of the complete radiation shield amounts to 100 cm at the inboard side. Fig. 1 shows a radial-poloidal cross section of the sector model used in the calculations. Fig. 2 shows the corresponding radial-toroidal cross-section at the inboard side of the torus mid-plane.

The neutron and photon radiation penetrating the shield causes various radiation damages at the superconducting magnet, among which those of the Epoxy insulator, leading to a weakening of its mechanical strength, are the most severe ones /Mau 85/.

In the present work, the superconducting magnet is represented by a homogeneous copper/steel-mixture, while the Epoxy insulator is treated in a

specific thin layer at the entrance of the superconducting magnet in order to obtain the peaking values for the penetrating radiation.

According to /Ver 86/ the representation of the spatial plasma source distribution used earlier /Fi 87/ has been modified to allow a dependence of the triangularity on the plasma minor radius. The parametric representation of the plasma contour lines is as follows:

$$R = R_0 + a \cdot \cos(t + \delta \cdot \sin t) + e\,(1 - (a/A)^2)$$

$$z = E \cdot a \cdot \sin t \qquad 0 \leq t \leq 2\pi$$

$$\delta = \delta_0 \cdot a/A \qquad 0 \leq a \leq A$$

For the NET double null configuration there is:

$R_0 = 518$ cm (plasma major radius)

$A = 135$ cm (plasma minor radius)

$E = 2.037$ (Elongation)

$e = 16.2$ cm (excentricity)

$\delta_0 = 0.57$ (maximal triangularity)

R is the radial distance from the torus axis and z is the poloidal distance from the torus mid-plane.

The plasma source density distribution S (a) is given by / Ver86 /:

$$S(a) = (1 - (a/A)^2)^4 \qquad 0 \leq a \leq A$$

Fig. 1 includes the plasma contour map gained with this representation. Note that there is a smooth transition from an elliptical to a D-shaped plasma source distribution as the plasma minor radius is increasing.

4. Three-dimensional Shielding Calculations in the NET Double Null Configuration

4.1 Poloidal Variations

The concentration of the plasma source around the torus mid-plane leads to strong poloidal variations of the 14 MeV neutron current impinging onto the first wall: as the poloidal distance to the torus mid-plane increases the 14 MeV neutron current decreases; at the torus mid-plane the maximum value is reached (fig. 3). The use of a plane first wall at the inboard side even enhances the poloidal variation. For the NET double null configuration, the peaking factor

(defined as the ratio of the maximum value to the poloidal average value) of the 14 MeV neutron current at the inboard first wall is 1.82 (table I). Consequently, the radiation penetrating the blanket/shield configuration also is strongest at the torus mid-plane. But a priori it is not evident how strong the poloidal variations in the spatial region of the superconducting magnet really are, and, furthermore, how this is related to results from the one-dimensional shielding calculations.

These questions have been analyzed by means of Monte Carlo shielding calculations with MCNP in a three-dimensional torus sector model of NET, that has been presented in the preceding section. Fig. 1 shows a poloidal-radial cross-section of this model; Fig. 2 shows the corresponding radial-toroidal cross-section at the torus mid-plane: due to its toroidal symmetry only one half of a 7.5 ° sector has to be taken into account. Reflecting boundary conditions are applied at the lateral walls of the sector model.

Importance sampling with geometry splitting and Russian roulette has been applied to describe the neutron and photon transport through the blanket and the vacuum vessel. In this way about 20 tracks per source neutron in general are taken into account. Typically 50 000 to 100 000 source neutrons are generated in one shielding calculation. Thus, a sufficient statistical accuracy for the relevant physical quantities scored in the spatial region of the superconducting magnet is achieved: in case of poloidally averaged quantities the statistical error typically lies below 5 %, in case of local quantities it lies between 5 and 10 % in the most important region around the torus mid-plane and between 10 and 20 % in the rather unimportant regions around the top and the bottom of a torus sector. But the latter regions will be reanalyzed in more detail in section 4.2, as there is a strong correlation to the divertor shielding problem.

4.1.1 Neutron Flux Densities

Due to multiple scattering processes, the poloidal profile of the total and the fast neutron flux density at the first wall is somewhat flatter than that of the direct 14 MeV neutron current (see fig. 3). In fact, the peaking factor at the inboard first wall amounts to only 1.22 and 1.29 for the total and the fast neutron flux, respectively (table I). This also reflects into the peaking factor of 1.47 for the 14 MeV neutron flux density, which - in contrast to the direct 14 MeV neutron current - includes scattered, but within the given margin of 0.01 MeV non-degraded 14 MeV neutrons from all spatial directions. Note that, with respect to

the poloidal variation, the energy release rates and hence the power densities roughly show the same behaviour like the total neutron flux density.

The poloidal profiles, however, are strongly dependent on the radial position within the blanket/shield configuration: the poloidal profiles are pronounced the more, the larger is the blanket/shield depth. This is seen very clearly in the map of the poloidal profiles of the total neutron flux density (fig. 4). In fact, the poloidal peaking factor increases from 1.26 in the first wall region to 2.17 in the Epoxy layer in case of the total neutron flux and from 1.33 to 2.21, in case of the fast neutron flux (see also fig. 5 and tables I and II). For the power density the same behaviour is observed: the corresponding peaking factor increases from 1.4 to 2.3. In case of the 14 MeV neutron flux the increase of the poloidal peaking factor is even more pronounced: it varies from 1.56 in the first wall region to about 3.0 at the front of the vacuum vessel (at the rear of the vessel the 14 MeV neutron flux is too low to obtain reliable results for its poloidal distribution).

This behaviour again is due to the plasma source concentration around the torus mid-plane and the use of a plane first wall: as seen from the central plasma region, the neutron pathways in the blanket/shield configuration increase as the distance to the torus mid-plane increases. Therefore the attenuation of the neutron radiation increases as the poloidal distance to the mid-plane increases. Consequently the poloidal peaking factor increases with increasing blanket/shield depth. This effect is very pronounced for the 14 MeV neutron radiation, because it practically only consists of 14 MeV source neutrons, whereas it is somewhat relaxed for the total and fast neutron flux, because in these quantities neutrons are involved that are created within the blanket/shield (by slowing down and multiplication processes) and therefore tend to smooth out the poloidal distribution as it is imposed on the first wall.

4.1.2 Epoxy Radiation Dose

The radiation dose deposited in the Epoxy insulator is the most crucial issue with respect to the radiation damage of the superconducting magnet. According to the specifications by the NET team, the Epoxy radiation dose should not exceed $5 \cdot 10^8$ rad over the lifetime of NET /Net 85/.

In the following an integral operation time of one year is assumed for NET resulting in a total fluence of 1 MWa/m^2. In fact, the present strategy provides a fluence of only 0.8 MWa/m^2 /Cha 86/. It would be advantageous, however, to have a safety margin by a factor 2 - 3 in order to scope with a larger fluence

resulting from a possible higher fusion power or a stretched operation time. Anyway it should be kept in mind that the radiation dose limit of $5 \cdot 10^8$ rad is subjected to more precise specifications, because there is a large spread of the limits, as they are given by different authors (cf. e.g. /Kü 87/).

Taking one full power year and a fusion power of 600 MW (for the actual configuration this in fact results in an integral fluence of 1 MWa/m^2 on the average), a poloidally averaged radiation dose of $3.5 \cdot 10^8$ rad is obtained for the Epoxy insulator. Corresponding to the poloidal profile of the neutron flux density (and also the photon flux density), there is however a strong poloidal variation of the Epoxy radiation dose (fig. 6): at the torus mid-plane it amounts to about $8 \cdot 10^8$ rad. Thus there is a peaking factor of ca. 2.3 for the Epoxy radiation dose. Consequently, the Epoxy radiation dose limit of $5 \cdot 10^8$ rad is exceeded in the spatial region around the torus mid-plane, although it is kept on the poloidal average. This, of course, only holds for the blanket/shield configuration assumed here. Clearly, there are various ways to improve the shielding effectiveness of this configuration: e.g. by improving the design of the "canister breeding blanket" with respect to its shielding function or by improving the vacuum vessel design. Regarding the more general aspect, it is seen, that it could become necessary to improve the shielding effectiveness of the vacuum vessel in the spatial region around the torus mid-plane. Primarily this would mean to use a more effective shielding material than steel: when used together with a hydrogeneous material, providing the neutron slowing down, tungsten is the most effective shielding material /Gre 85/. But this would complicate the technical layout of the vacuum vessel considerably. In view of the rather uncertain radiation dose limits, it has to be analyzed carefully, if this really is necessary.rather uncertain radiation dose limits, it has to be analyzed carefully, if this really is necessary.

4.2 Radial Profiles

4.2.1 Neutron Flux Densities

Fig. 7 shows the radial profile of the poloidal averages of the total, the fast and the 14 MeV neutron flux densities. Due to the use of beryllium and the presence of a rather transparent "plenum zone" the decrease of the total and the fast neutron flux density within the blanket is very moderate: going from the first wall to the rear of the blanket, the total flux only decreases by a factor of 4 and the fast neutron flux correspondingly by a factor of 4.5. Consequently the "canister breeding blanket" cannot claim to perform the function of a shielding

blanket very well. From this point of view its design could be improved, primarily by putting some more shielding material (e.g. steel) into the plenum zone and by adding some hydrogeneous material at the back of the breeding zone.

The 14 MeV neutron flux, on the other hand, decreases very fast: typically by a factor of about 300, if the energy margin taken into account around 14 MeV is very sharp, or by a factor of about 60, if the energy margin is taken very broad (13.5 - 14.9 MeV, i.e. the source energy group of the 100 GAM II group structure). Anyway, at the back of the blanket the 14 MeV neutron flux is about two orders of magnitude smaller than the total neutron flux.

Passing through the vacuum vessel, the 14 MeV neutron flux decreases further by about 4 - 5 orders of magnitude. An average mean free path of ca. 7 cm can be deduced from the exponential decrease of the 14 MeV neutron flux in the region of the vacuum vessel. This is in agreement with the same quantity estimated from the inelastic scattering cross section of iron. At the rear of the vacuum vessel the 14 MeV neutron flux is about 3 orders of magnitude smaller than the total neutron flux. Consequently it only plays a minor role with respect to the radiation damage of the superconducting magnet.

Across the vacuum vessel the total and the fast neturon flux decrease by nearly 4 orders of magnitude (fig. 7), demonstrating the function of the vacuum vessel as efficient radiation shield.

The ratio of the fast to the total neutron flux Φ_{fast}/Φ_{tot} varies rapidly with the radial position through the blanket/shield configuration (fig. 8): it is about 55 % in the first wall region and 25 % in the Epoxy layer. The actual value of course strongly depends on the specific material composition. In the spatial region of the vacuum vessel, Φ_{fast}/Φ_{tot} is very low in the water layers (typically 20 %), but considerably higher in the steel plates (typically 50 % at the front of the vessel and 35-40 % at the rear). Consequently, water is superior to steel as neutron slowing down medium in the region of the vacuum vessel, whereas the opposite is true in the first wall region. This behaviour is due to the different kinds of the nuclear reactions that are responsible for the neutron slowing down in water and steel, in correlation with the energy distribution of the neutrons.

In the case of water, the neutrons are slowed down through elastic scattering processes on hydrogen. However, above ca. 0.1 MeV the corresponding cross-section decreases continuously with increasing energy. At 14 MeV it is only ca. 0.3 barn. In the case of steel, the neutrons are slowed down through inelastic scattering processes on the steel components (primarily iron). The reaction thresholds of the inelastic neutron scattering on the steel components typically

lie around 1 MeV. Hence steel cannot act as neutron slowing down medium, if the neutron spectrum is concentrated below 1 MeV: this, in fact, is the case in the region of the vacuum vessel. If, however, the neutron spectrum is concentrated above several MeV, as it is the case in the first wall region, the inelastic scattering cross-section of steel becomes larger than the elastic scattering cross-section of water. Consequently, steel is a more efficient neutron slowing down medium than water in the first wall region.

These observations of course agree with systematic shield optimization studies /Gre 85/, showing that in case of a simple iron/water shield, the water fraction should increase continuously, from zero in the first wall region to a maximal value of about 30 % at the centre of the shield. For larger distances to the first wall, the water fraction should decrease again: this is due to the function of the back of the shield as photon radiation attenuator.

4.2.2 Power Density

The radial power distribution over the blanket/shield configuration corresponds to the radial profile of the total neutron flux density: the decrease within the blanket is moderate, but it is considerable larger across the vacuum vessel (fig. 9). Typically the power density is about 9 W/cm^3 (peaking value) in the first wall region and about 1 mW/cm^3 (peaking value) in the rear of the vacuum vessel. In the Epoxy insulator the peaking power density is about 0.4 mW/cm^3. The corresponding poloidally averaged quantities are 6.4 W/cm^3, 0.59 mW/cm^3 and 0.2 mW/cm^3, respectively.

In the blanket region, the power release mainly is due to neutron induced nuclear reactions (primarily the Li^6 (n, α)t-, the Be (n, 2n)2α - reactions and elastic scattering processes), whereas in the region of the vacuum vessel - consisting essentially of steel plates - it is mainly due to the absorption of the photon radiation in the steel components (fig. 10). In the water layers between the steel plates again the neutron induced reactions are responsible for the energy release: either through elastic scattering processes on hydrogen (no boron present) or through the neutron absorption in B^{10} (boron acid present).

The energy released in the Epoxy insulator, which in effect gives the radiation dose, is due to neutron reactions to 54 % and to photon absorptions to 46 %. More than 90 % of the neutron radiation dose of the Epoxy insulator is due to fast neutrons. Consequently, the Epoxy radiation dose can be decreased further by decreasing the fast neutron flux and the photon radiation. Both effects can be

achieved by decreasing the steel fraction and increasing the borated water fraction at the back of the vacuum vessel. Since steel not only acts as photon attenuator, but primarily as photon emitter, it would be beneficial in this respect to replace it, at least partially, by a more effective photon attenuator, e.g. lead.

4.3 Relations Between One- and Three-dimensional Calculations

It is of special interest to know the relations between one- and three-dimensional shielding calculations, since the first ones most often are used in shielding analyses. Note, however, that the one-dimensional calculations presented here, also are performed with the Monte Carlo method, i.e. with the help of the MCNP-code. Concerning the relations between deterministic one-dimensional and probabilistic three-dimensional calculations, it is recalled that deterministic shielding calculations using group nuclear data tend to underestimate the radiation penetrating the shield (see section 2).

At the first wall, the one-dimensional value of the impinging 14 MeV neutron current agrees very well with the poloidally averaged one (fig. 3 and table I), while for the total and the fast neutron flux density, the one-dimensional values agree very well with the three-dimensional peaking values at the torus mid-plane. This agreement primarily results from a suitable chosen one-dimensional model of the torus and the plasma source (see ref. /Fi 87/ for more details). It seems to be a specific feature of the NET double null configuration, that the quantitative agreement nearly is perfect.

Passing the blanket and the vacuum vessel, the relations between one- and three-dimensional neutron flux densities as they are observed in the first wall region, no longer hold: In general, the one-dimensional neutron fluxes agree roughly with the poloidally averaged ones (figs. 11, 12). In the Epoxy layer e.g the one-dimensional total neutron flux is only 20 % higher than the poloidally averaged one, but it is about 70 % lower than the peaking value at the mid-plane (table III). Consequently, the one-dimensional calculation underestimates the peaking values of the penetrating radiation at the torus mid-plane, although it is able, on the other hand, to reproduce the peaking values (for the neutron fluxes as for the power densities) in the first wall region! Concerning the Epoxy radiation dose, this underestimation roughly amounts to a factor of 2 (see also fig. 6). It is pointed out, that the actual relation between one- and three-dimensional values strongly depends on the radial position in the blanket/shield configuration.

4.4 Divertor Shielding

The KfK-design of a helium cooled divertor provides a 25 mm thick molybdenum plate protected by a 5 mm thick graphite layer /Da 86/. The divertor plate is backed by a steel structure providing the radiation shielding and the divertor support, and enclosing the helium supply pipes. For evaluating the shielding performance of the steel structure, it is sufficient to restrict the analysis to the upper poloidal divertor in the NET double null configuration. Hence the geometrical model is restricted to the upper poloidal half of a torus sector by applying a reflective boundary condition at the torus mid-plane (fig. 13). In this way the shielding calculation can be performed without methodical restrictions but with reduced expense with respect to the computing times needed.

For the shielding analyses, the total thickness of the steel structure and the divertor plate has been fixed at 35 cm which is the total thickness of the inboard blanket segment. The steel fraction of the structure, however, has been varied from ca. 20 % to ca. 60 %, corresponding to effective steel thicknesses of 7 to 19 cm, respectively.

Again importance sampling with geometry splitting and Russian roulette has been applied in order to follow the neutron and photon tracks through the divertor steel structure and the vacuum vessel. Typically 50 000 neutron histories are taken into account in one divertor shielding calculation, consuming 4 to 6 h CPU in general. The statistical accuracy for the relevant physical quantities scored in the spatial region of the superconducting magnet is in the order of 10 %.

The upper divertor is subjected to an average 14 MeV neutron current, that is roughly one half of the corresponding poloidally averaged value at the inboard first wall (see fig. 3). In terms of the neutron wall load, it is 0.35 MW/m^2 on the average at the divertor and 0.70 MW/m^2 on the average at the inboard first wall.

There is a discontinuity at the junction of the inboard first wall and the divertor due to the incline of the divertor towards the plasma centre. In case of the 14 MeV neutron current this discontinuity amounts to a factor 2. The poloidal variation of the 14 MeV neutron current at the divertor is rather strong (fig. 3): maximal and minimal values differ by a factor 2.3 (table IV).

The same qualitative behaviour can be observed in case of the total and the fast neutron flux density at the divertor but due to the inclusion of multiple scattered neutrons in these quantities, the corresponding poloidal profiles are smoothed out to some extent (fig. 3). In case of the total neutron flux density, the poloidally averaged values for the first wall and the divertor differ by only 30 %,

in case of the fast neutron flux density by 40 %. The discontinuity at the junction of the first wall and the divertor only amounts to ca. 10 % in case of the total and to about 20 % in case of the fast neutron flux. Maximal and minimal values at the divertor differ by 40 % in case of the total neutron flux and by 46 % in case of the fast neutron flux.

Within the divertor supporting structure, the poloidal variation of the neutron flux densities increases with increasing depth (fig. 14) due to the fact, that the neutron pathways - as seem from the plasma centre - increase with the poloidal length. At the front of the vacuum vessel behind the divertor, the poloidal profile of the total neutron flux, however, is smoothed out nearly completely (fig. 15). This of course is a geometrical effect: it is due to the increasing incline of the vacuum vessel with increasing poloidal length, i.e. the bending of the vacuum vessel (see fig. 13).

Within the vacuum vessel, the poloidal profile again changes with depth, depending crucially on the effective thickness of the divertor steel structure (figs. 15, 16). In case of an effective thickness of 19 cm, the neutron flux density behind the vacuum vessel is decreasing continuously with increasing poloidal length (fig. 16), although at the front of the vacuum vessel it is slightly increasing in the divertor region (fig. 15). This again can be traced back to the fact that the neutron pathways, as seen from the plasma centre, are increasing with increasing poloidal length.

In the case, however, that the effective thickness of the divertor steel structure is reduced (to 13 or 7 cm), the neutron flux impinging on to the front of the vacuum vessel is enhanced in such a way, that behind the vacuum vessel it is no longer decreasing with the poloidal length, but raher increasing (fig. 16). In the case, that the effective thickness of the divertor steel structure in only 7 cm thick, the peaking value of the neutron flux density even is reached in the upper part of the bended vacuum vessel (cf. figs. 16 and 13). This behaviour indicates, that there is a shift for the minimal neutron pathways, depending on the effective thickness of the divertor steel structure. In the latter case, the minimal neutron pathways are obtained in the upper part of the bended vacuum vessel, which means, that there most of the neutrons impinge perpendicularly on the front of the vessel.

For the calculation of the Epoxy Radiation dose again one full power year of operation is assumed. Regarding the shielding effectiveness of the divertor steel structure, three different cases are compared: an effective thickness of the steel

structure of 19, 13 and 7 cm corresponding to a steel fraction of 60, 40 and 20 %, respectively.

Fig. 17 shows the poloidal profile of the Epoxy radiation dose for the three cases. The qualitative behaviour of course is the same as that of the neutron flux densities discussed above. With respect to the quantitative level it is observed, that the Epoxy radiation dose in the region behind the divertor is equal or less than it is in the upper region behind the blanket, if the steel content of the divertor structure is not less than 40 %. If it is less than 40 %, there is again an increase of the Epoxy radiation dose in the region behind the divertor. In the case that the steel fraction of the divertor structure is 20 %, the peaking value in the divertor region is about $5 \cdot 10^8$ rad (fig. 17), i.e. the limiting value. Note, however, that the peaking value of the Epoxy radiation dose at the torus mid-plane under the same conditions is larger by ca. 70 %.

5. Neutron Streaming Through the Gaps Between Neighbouring Blanket Segments: Two-Dimensional Shielding Calculations

The blanket segments of NET have to be seperated by a gap of at least 20 mm in toroidal direction in order to be isolated electrically against each other. Furthermore, a gap between neighbouring segments also is requested to facilitate the maintenance of the blanket segments. As a consequence, there will be a considerable neutron streaming through the segment gaps and the vacuum vessel directly is subjected to an unshielded neutron flux at the bottom of the gaps.

The impact of the neutron streaming through the segment gaps on the shielding performance of the vacuum vessel has been analysed in a two-dimensional approach. A 7.5 ° torus sector is modelled in cylindrical geometry with the torus axis as symmetry axis. In fact, this two-dimensional sector model is equivalent to the usual one-dimensional model in cylindrical geometry, if the toroidal segmentation (i.e. the insertion of the segment gap and the segment walls) would not be performed. Inboard and outboard sectors are taken into account in the usual way in this model. At the inboard side, a segment gap and segment walls are inserted in the mid-plane of the 7.5 ° sector (fig. 18). Thus, the 7.5 ° - sector, treated in the calculations, reaches from the mid-plane of one real torus segment to the next one by taking into account the separating gap and the side walls of the blanket segments.

The width of the gap between neighbouring toroidal segments, that has been used in the calculations, is 25 mm. Thus the segment gap covers 5.2 % of the inboard first wall area. The depth of the gap is 35 cm, i.e. the total thickness of the inboard blanket.

Again importance sampling with geometry splitting and Russian roulette has been applied to follow the neutron and photon tracks through the blanket segments, the gap in between, and the vacuum vessel. Typically 30 000 to 60 000 neutron histories are taken into account in one shielding calculation, assuring a statistical accuracy of about 5 % on the average for the relevant physical quantities scored in the spatial region of the superconducting magnet. The computing times needed in general reach from 2 to 4 h CPU.

5.1 Segment Gap

Fig. 19 compares the total, the fast and the 14 MeV neutron flux in the gap and the blanket as a function of the radial position. The neutron flux densities in the blanket in this case refer to a 1d-description of a torus sector (i.e. no gap and no segment walls included). It is observed, that the total neutron flux in the graphite tiles of the first wall agrees very well with the corresponding one in the segment gap. At the bottom of the gap, the total flux is about 33 % higher than behind the blanket (in a 1d-description). In case of the fast neutron flux ($E > 0.1$ MeV), there is already a difference of 5 % in the first wall region (this is due to neutron slowing down processes in the graphite tiles) and again 31 % at the bottom of the gap. The strongest streaming effect obviously has to be expected in case of the 14 MeV neutron flux. In fact, in the first wall region it is already 30 % higher than the corresponding flux in the blanket; at the bottom of the gap there is a difference by a factor of 4.

Going from the first wall region to the rear of the blanket, the 14 MeV neutron flux decreases by a factor of 24 in the segment gap and by a factor 78 in the blanket. The corresponding factors for the fast and the total neutron fluxes are 4.3 and 3.7 in the gap, 5.3 and 5.0 in the blanket, respectively.

5.2 Impact on the Shielding Performance of the Vacuum Vessel

There are two effects of the neutron streaming through the segment gap on the shielding performance of the vacuum vessel: firstly, in toroidal direction there is a peaking of the neutron flux at the bottom of the segment gap; secondly, there

is a lifting of the level of the neutron flux over the whole toroidal segment, i.e. not only at the bottom of the segment gap but also behind the blanket segment.

Thus, in case of taking into account the segment gap, the toroidally averaged neutron flux densities are higher than the corresponding values in the 1d-description. At the front of the vacuum vessel this difference amounts to about 20 % for the total and 16 % for the fast neutron flux. At the rear of the vacuum vessel the corresponding values are 15 % and 11 %, respectively. In case of the 14 MeV neutron flux the difference is about 50 % at the front and around 15 % at the rear of the vacuum vessel. But acutally, in the spatial region of the vacuum vessel the 14 MeV neutron flux only plays a minor role: it is only about 1 % of the total neutron flux at the front, and it is roughly three orders of magnitude smaller than the total neutron flux at the rear of the vacuum vessel (cf. sec 4.2.1).

At the front of the vacuum vessel the toroidal peaking factors amount to ca. 1.13 for the total and 1.15 for the fast neutron flux. Therefore the toroidal profile of the neutron flux is rather flat (see also fig. 20) and furthermore, the peaking of the flux is restricted to a spatially small region (fig. 20). Consequently, the toroidal profile flattens completely, as the depth of the vacuum vessel increases: the peaking factor reaches already its asymptotic value 1.0 behind the first steel plate of the vacuum vessel, which is 11 cm thick (fig. 21).

In case of the 14 MeV neutron flux density, the toroidal profile at the front of the vacuum vessel is pronounced strongestly (fig. 20): the peaking factor amounts to ca. 2.8. But again, this is of minor importance, because already there the 14 MeV neutron flux is only about 1 % of the total one and it decreases further very rapidly.

The main effect of the neutron streaming through the segment gap on the vacuum vessel consequently is not a toroidally peaking, but a smooth lifting of the neutron fluxes by about 20 % on the average (see also fig. 22).

Consequently, there is also no toroidal variation in the spatial region of the superconducting magnet due to the impact of the segment gaps. This holds for the neutron flux densities as for the Epoxy radiation dose: the toroidal profiles are completely flat. Again, there is a lifting of the corresponding levels: ca. 18 % for the total, ca. 14 % for the fast neutron flux and ca. 15 % for the Epoxy radiation dose.

Summing up, it can be stated, that the impact of the neutron streaming through the segment gaps on the shielding performance of the vacuum vessel is rather moderate. There is a slight lifting of the level of the penetrating radiation in the

spatial region of the superconducting magnet, but no toroidal variations can be observed.

Clearly, the effects observed will be enhanced by increasing the gap width (e.g. 4 cm are under discussion for NET) and the gap depth (e.g. 65 cm at the outboard side). But it can be concluded from these calculations, that the effect of the segment gaps on the shielding performance of the vacuum vessel is considerably smaller than the effect of the poloidal peaking of the neutron flux densities at the torus mid-plane (cf. section 4.1).

6. Conclusion

Multi-dimensional shielding calculations, based on the application of biased Monte Carlo techniques with the help of the MCNP code, have been performed in the NET double null configuration to evaluate the effectiveness of the shielding components in a geometrical description that is very close to reality.

The main objects of the analysis have been the evaluation of the poloidal variations of the physical quantities relevant for the radiation shielding, the shielding performance of the divertor, the impact of the neutron streaming through segment gaps on the shielding performance of the vacuum vessel and the relations between one- and three-dimensional shielding calculations.

The most important issues of the analysis can be stated as follows:

- At the inboard side of the NET torus, the poloidal peaking factors increase as the distance to the first wall is increasing. The peaking factor for the Epoxy radiation dose amounts to about 2.2, whereas the peaking factor of the power density in the first wall region is about 1.4.
- The relation betwen a one-dimensional and a three-dimensional treatment of the shielding problem is strongly dependent on the radial position. In case of the neutron flux density e.g., the one-dimensional value agrees with the three-dimensional peaking value in the first wall region, but the one-dimensional value agrees with the poloidally averaged one if the distance to the first wall increases. In the spatial region of the superconducting magnet the one-dimensional value for the neutron flux density as for the Epoxy radiation dose typically is lower than the peaking value at the torus mid-plane by a factor of 2.
- Deterministic shielding calculations using (unshielded) group nuclear data underestimate the penetrating neutron and photon radiation. For the NET

shielding configuration, this underestimation roughly amounts to a factor of 2. Consequently, a one-dimensional deterministic shielding calculation, performed in the mid-plane of the torus, has to be corrected by a factor of 4, in order to take into account the maximally penetrating radiation.

- The impact of the neutron streaming through segment gaps on the shielding performance of the vacuum vessel is rather moderate. In the spatial region of the superconducting magnet, there is a slight lifting of the penetrating radiation by about 20 % on the average. But there is no toroidal variation due to the segment gap, as it is the case at the front of the vacuum vessel.
- The shielding performance of a helium cooled divertor steel structure is sufficient, if the effective thickness of the steel structure is on the order of 10 to 15 cm.

7. References

/Bo 87/ W.F. Bogaerts, M.J. Embrechts, R. Waeben: Application of the Aqueous Self-Cooled Blanket Concept to a Tritium Producing Shielding Blanket for NET, EUR-FU-12-80-87-75 (1987).

/Bri 86/ J.F. Briesmeister (Ed.): MCNP - A General Monte Carlo Code for Neutron and Photon Transport, Version 3A, LA-7396-M, Rev. 2, Sept. 1986.

/Cha 86/ M. Chazalon, B. Libin: Strategy of Breeding Blanket Introduction in NET and Testing Requirements, 14th Symp. Fus. Techn., 8 - 12 Sept. 1986, Avignon, France, Proc. pp. 409 - 415.

/Dä 87/1/ W. Dänner: Shielding Blankets and their Nuclear Performance, NET/87/IN-021, 11.6.1987.

/Dä 87/2/ W. Dänner: The Shielding Properties of the Vacuum Vessel, NET/87/IN-022, 16.6.1987.

/Dal 87/ M. Dalle Donne, U. Fischer, G. Sordon, E. Bojarski, H. Reiser, P. Norajitra, E. Bogusch: Pebble Bed Canister, a Ceramic Breeder Blanket with Helium Cooling for NET, 14th Symp. Fus. Technology, 8 - 12 Sept. 1986, Avignon, France, Proc. pp 423 - 428.

/Fi 87/ U. Fischer: Multi-dimensional Neutronics Analysis of the "Canister Blanket" for NET, KfK-4255 (1987).

/Fi 88/ U. Fischer: Analysis of a Benchmark for the Penetration of 14-MeV Neutrons in Iron: Deterministic vs. Probabilistic Computational Procedure, to be published.

/Gre 85/ E. Greenspan, P. Levin, A. Kinrot: Optimal Shield Concepts for Experimental Fusion Devices, Fusion Technology 8 (1985), 1026 - 1031.

/Kü 87/ M. Küchle, E. Bojarski, S. Dorner, U. Fischer, J. Reimann, H. Reiser: Potential and Problems of an Aqueous Lithium Salt Solution Blanket for NET, KfK-4271 (1987).

/Mau 85/ W. Maurer: Neutron and Gamma Irradiation Effects on Organic Insulating Materials for Fusion Magnets, KfK-3974 (1985).

/Net 85/ Next European Torus, Status Report 1985, NET Report 51, CEC Brussels 1985.

/Ver 86/ K.A. Verschuur: Poloidal Variation of the NET Blanket Nuclear Response Functions, ECN-87-001 (1987).

	3d-calculation		1d-calculation
	poloidally averaged	at the mid-plane	
Φ_{tot} [10^{14}cm^{-2}s^{-1}]	3.66	4.48	4.76
Φ_{fast} [10^{14}cm^{-2}s^{-1}]	2.12	2.73	2.72
Φ_{14} [10^{13}cm^{-2}s^{-1}]	5.76	8.48	
J_{14} [10^{13}cm^{-2}s^{-1}]	3.10	5.62	3.03

Table I: Neutron flux densities and 14 MeV neutron current (J_{14}) impinging onto the inboard first wall

	3d-calculation		1d-calculation
	poloidally averaged	at the mid-plane	
Φ_{tot} [10^{14}cm^{-2}s^{-1}]	3.58	4.50	4.38
Φ_{fast} [10^{14}cm^{-2}s^{-1}]	1.99	2.65	2.36
Φ_{14} [10^{13}cm^{-2}s^{-1}]	4.04	6.29	4.49

Table II: Neutron flux densities within the carbon tiles of the inboard first wall

	3d-calculation		1d-calculation
	poloidally averaged	at the mid-plane	
Φ_{tot} [10^{10}cm^{-2}s^{-1}]	1.93	4.06	2.35
Φ_{fast} [10^{10}cm^{-2}s^{-1}]	0.47	1.02	0.58

Table III: Neutron flux densities within the Epoxy insulator

	J_{14} [10^{13}cm^{-2}s^{-1}]	Φ_{tot} [10^{14}cm^{-2}s^{-1}]	Φ_{fast} [10^{14}cm^{-2}s^{-1}]
average value	1.54	2.69	1.53
maximal	2.24	3.12	1.81
minimal	1.91	2.26	1.24

Table IV: Neutron flux densities and 14 MeV neutron current impinging onto the upper poloidal divertor

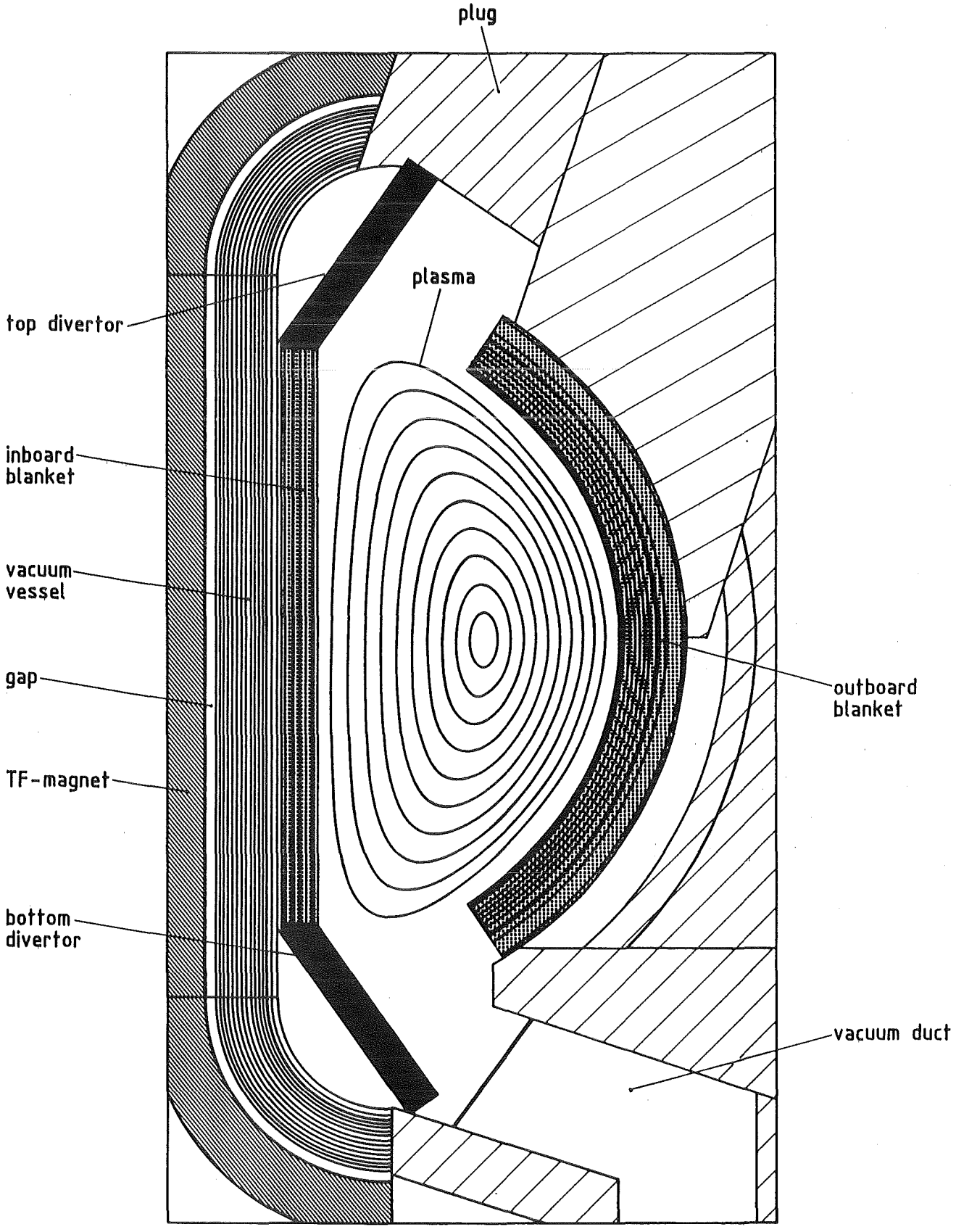

Fig. 1 Radial-poloidal cross-section of the torus sector model, including the plasma source contour map, used in the Monte Carlo calculation.

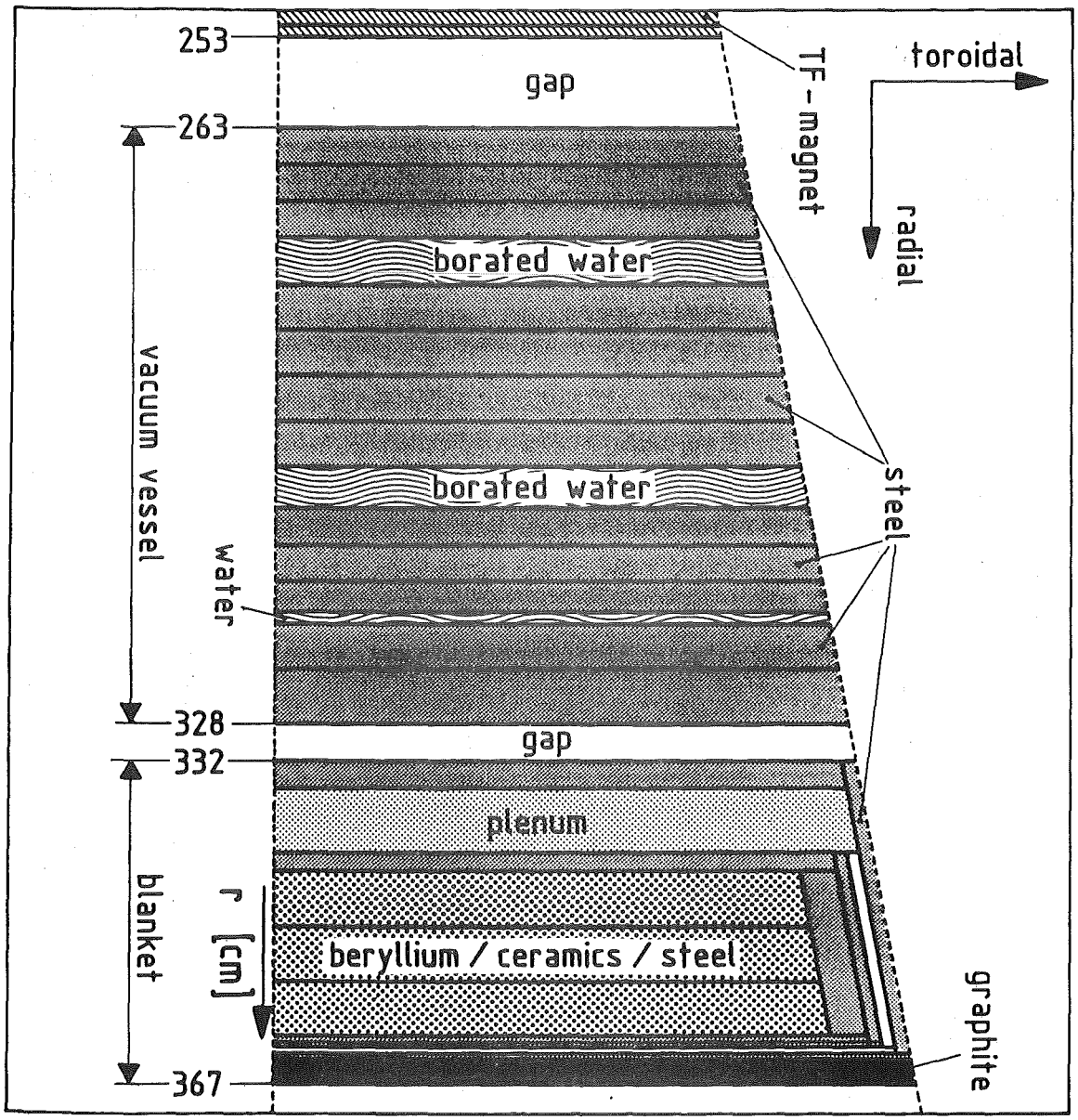

Fig. 2 Radial-toroidal cross-section of the inboard segment in the torus mid-plane.

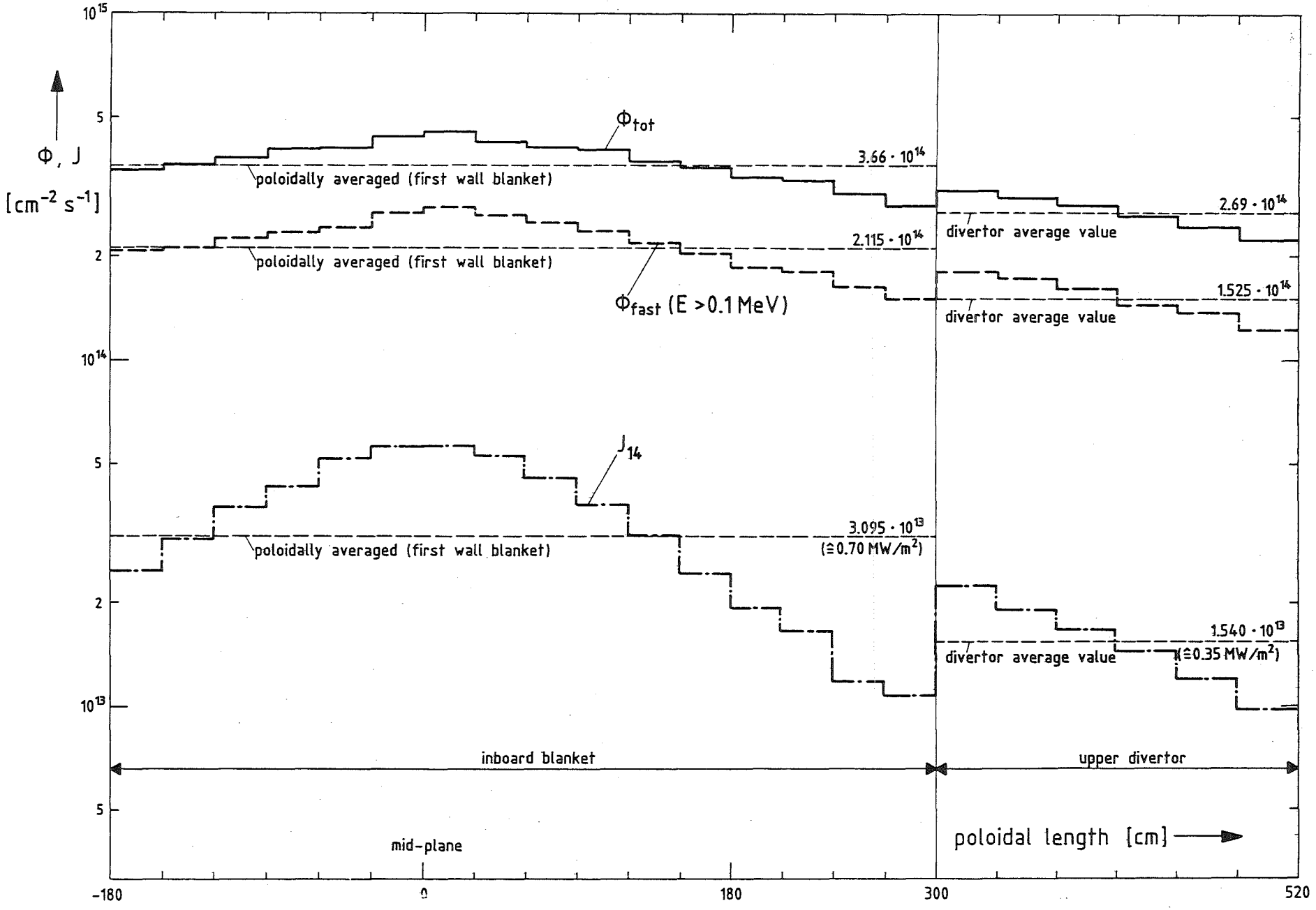

Fig. 3 Poloidal profiles of the direct 14 MeV neutron current (J_{14}), the total (Φ_{tot}) and the fast (E>0. 1 MeV: Φ_{fast}) neutron flux densities at the inboard first wall and the upper divertor.

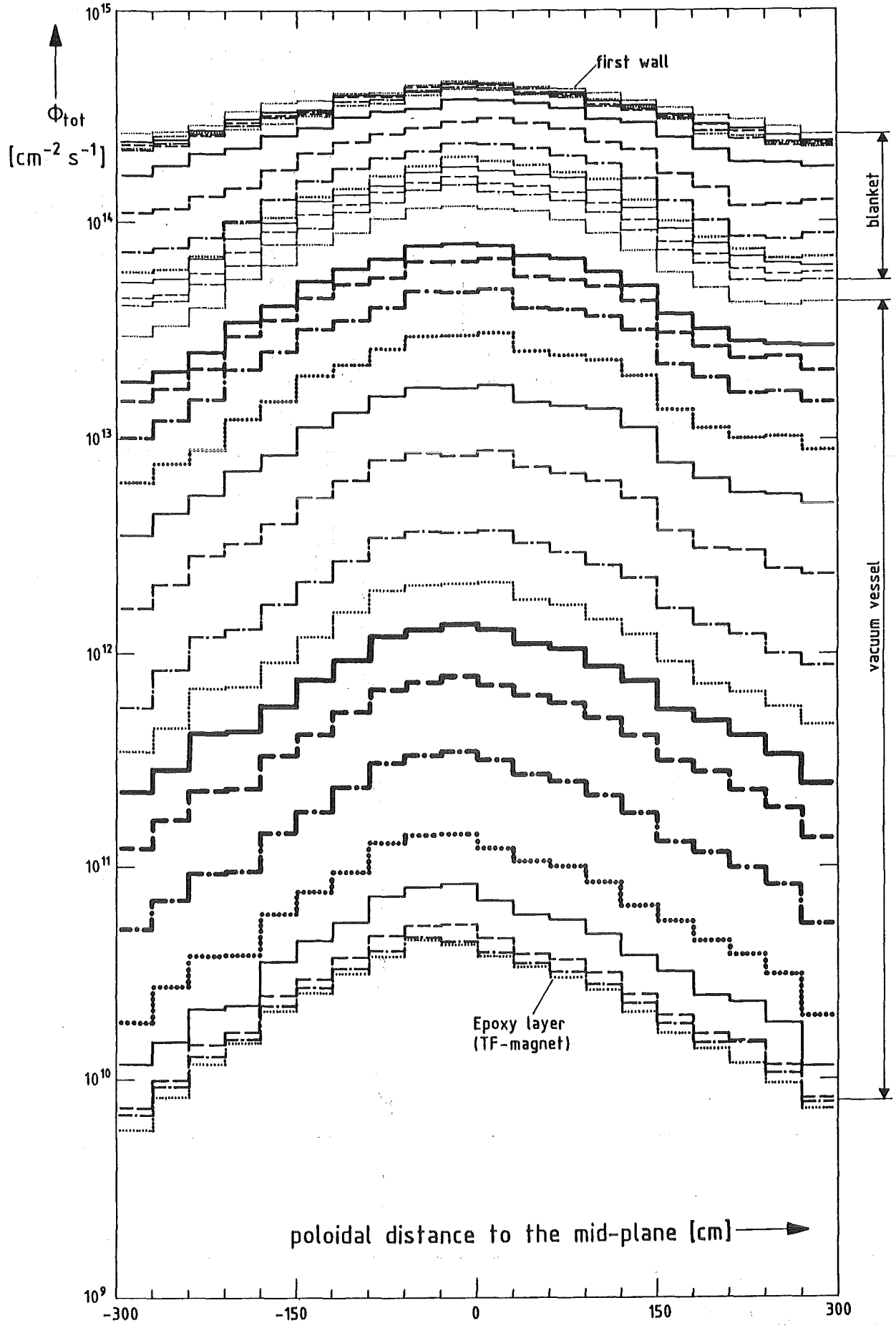

Fig. 4 Poloidal profiles of the total neutron flux density dependent on the radial position in the inboard segment.

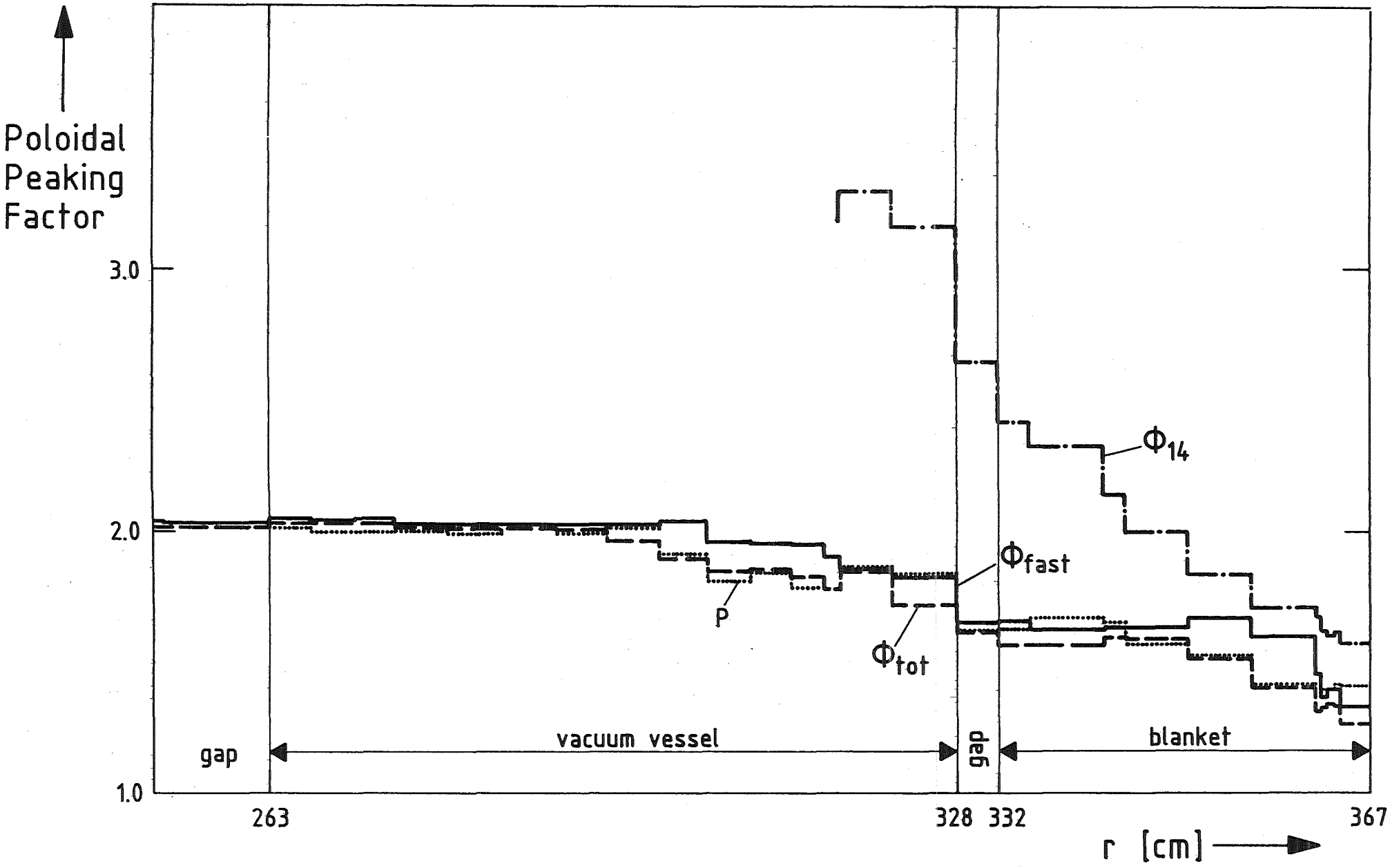

Fig. 5 Radial profiles of the poloidal peaking factors.

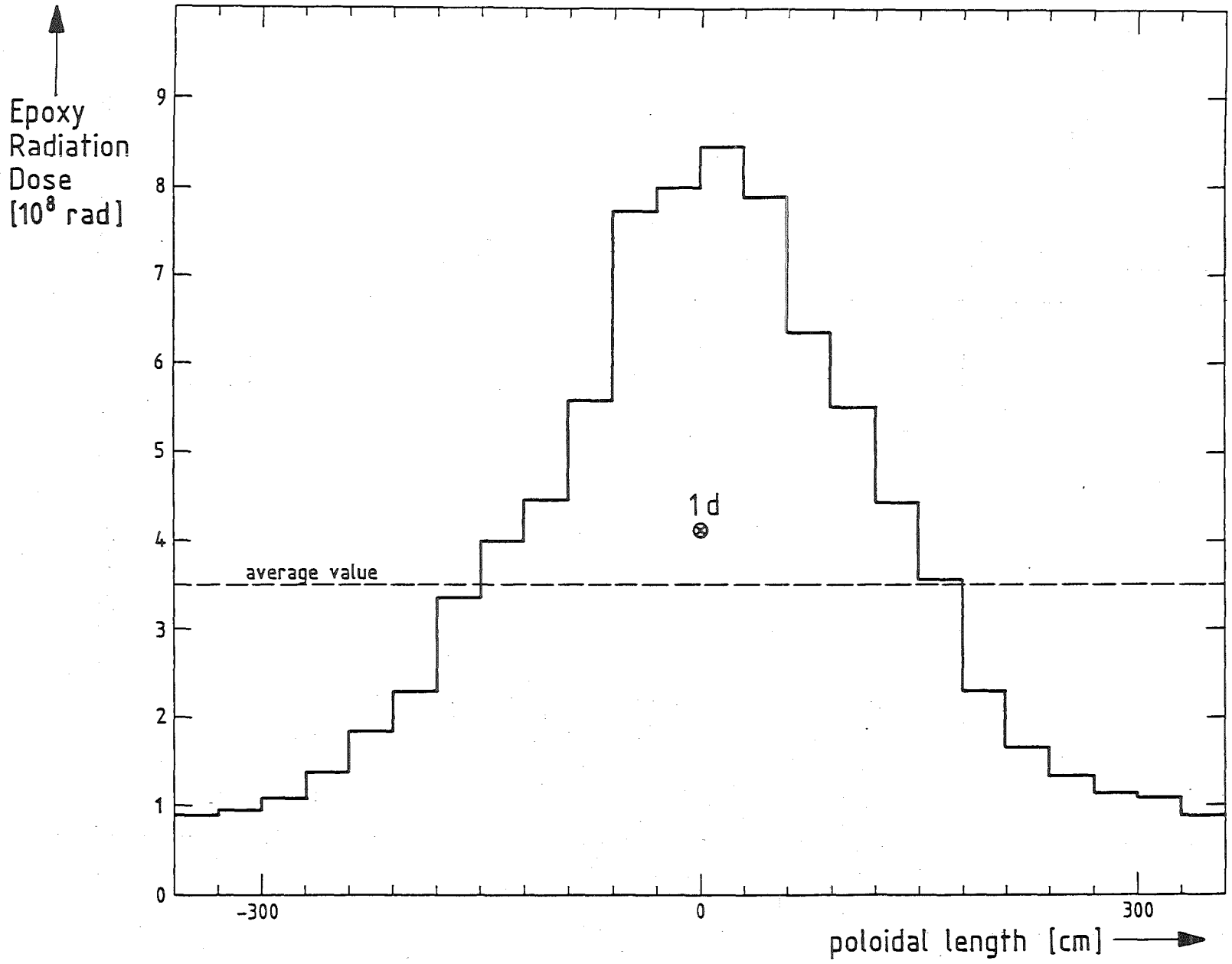

Fig. 6 Poloidal profile of the Epoxy radiation dose.

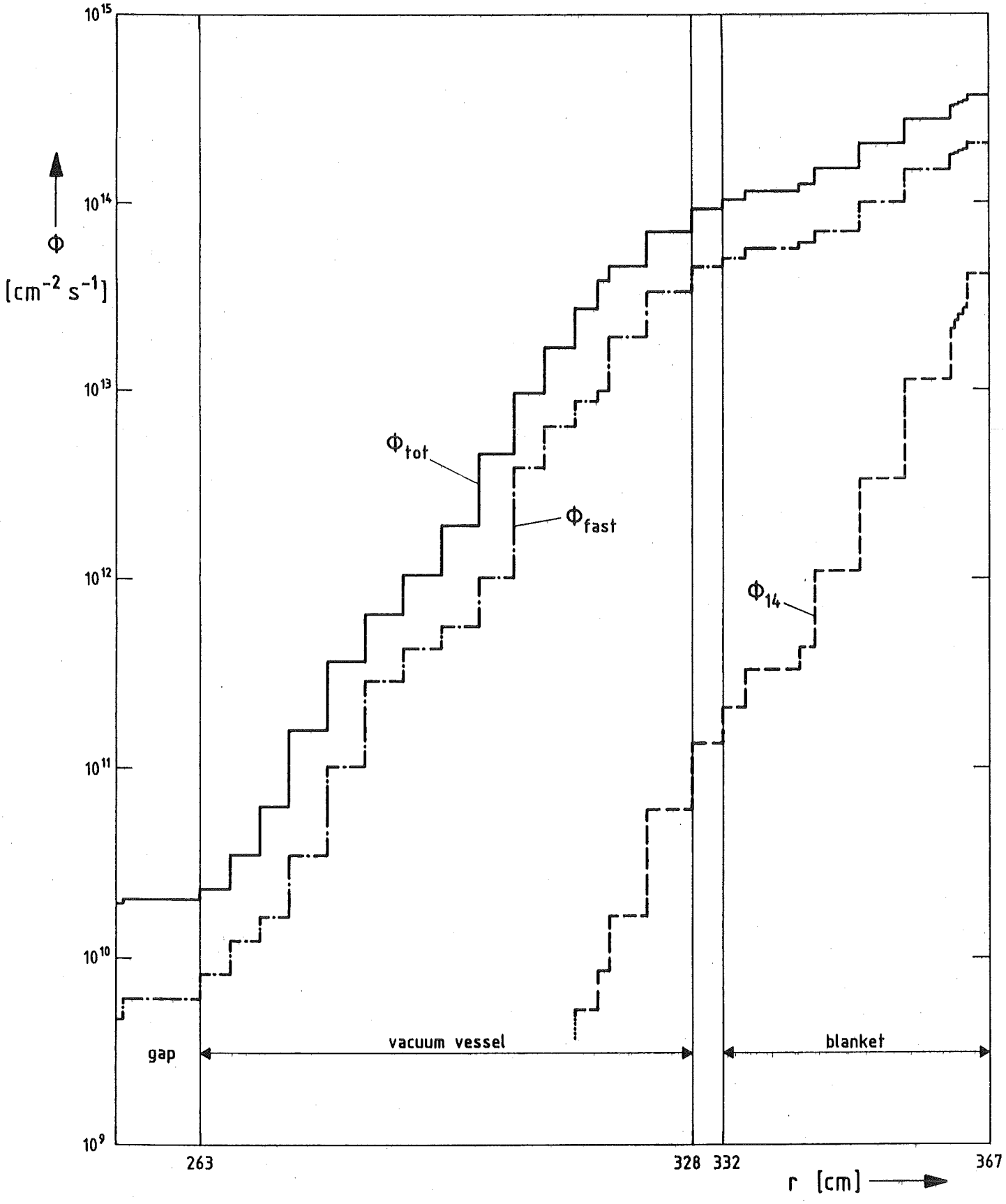

Fig. 7 Radial profiles of the total (Φ_{tot}), the fast (Φ_{fast}) and the 14-MeV (Φ_{14}) neutron flux densities (poloidal averages).

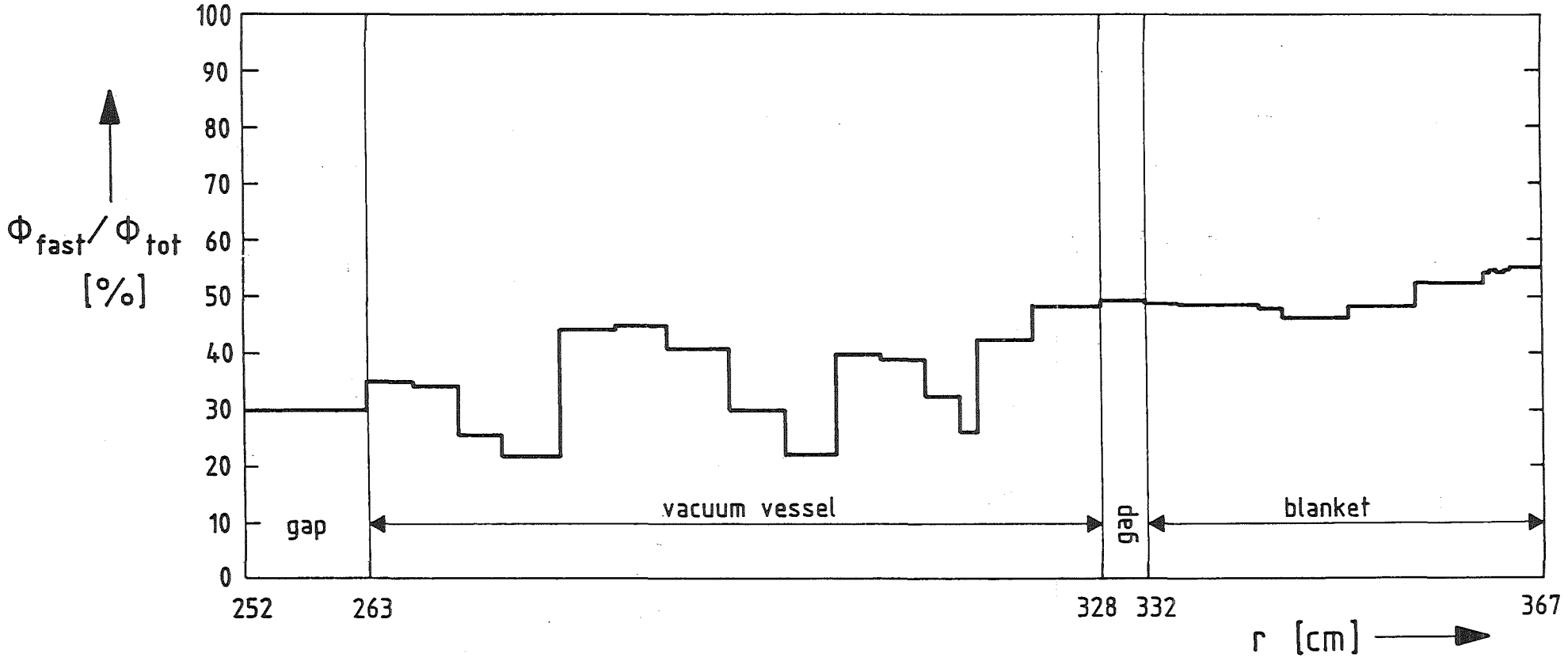

Fig. 8 Radial profile of the ratio ϕ_{fast}/ϕ_{tot} (fast to total neutron flux density).

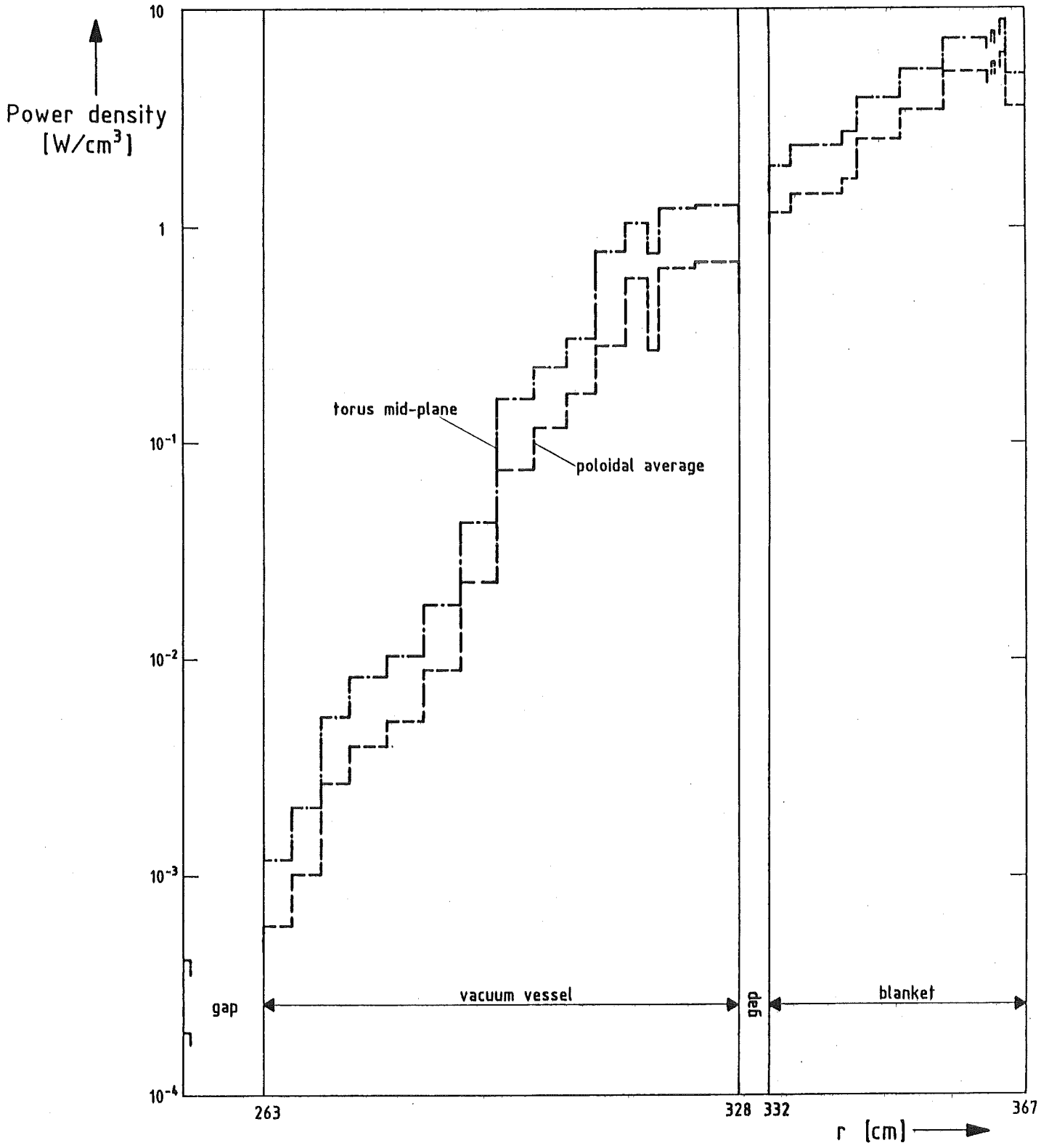

Fig. 9 Radial profile of the power density: poloidal average and peaking value in the torus mid-plane.

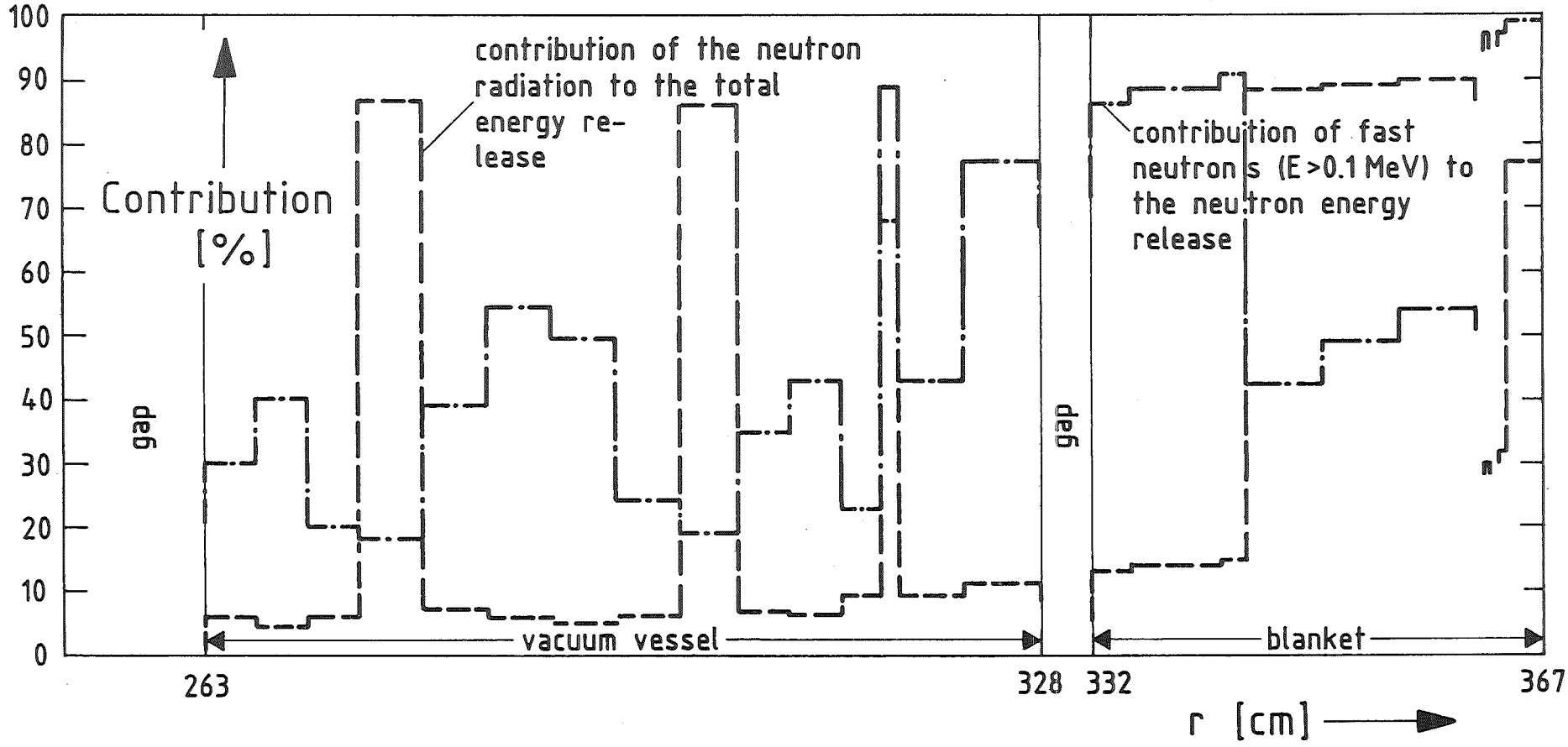

Fig. 10 Radial profile of the neutron contribution to the energy release and its contribution from fast (E>0.1MeV) neutrons.

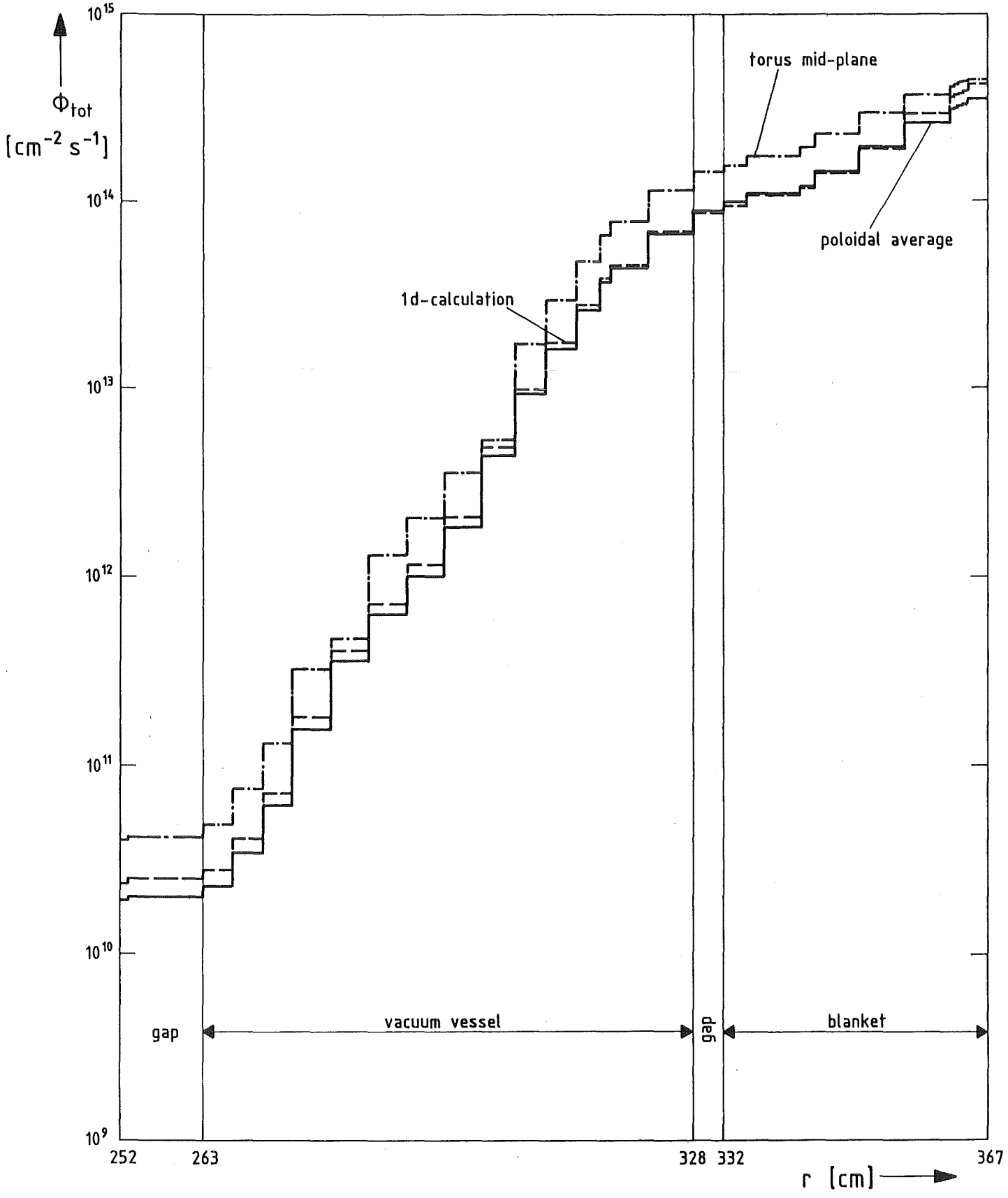

Fig. 11 Radial profile of the total neutron flux density: poloidal average, peaking value in the torus mid-plane and one-dimensional value.

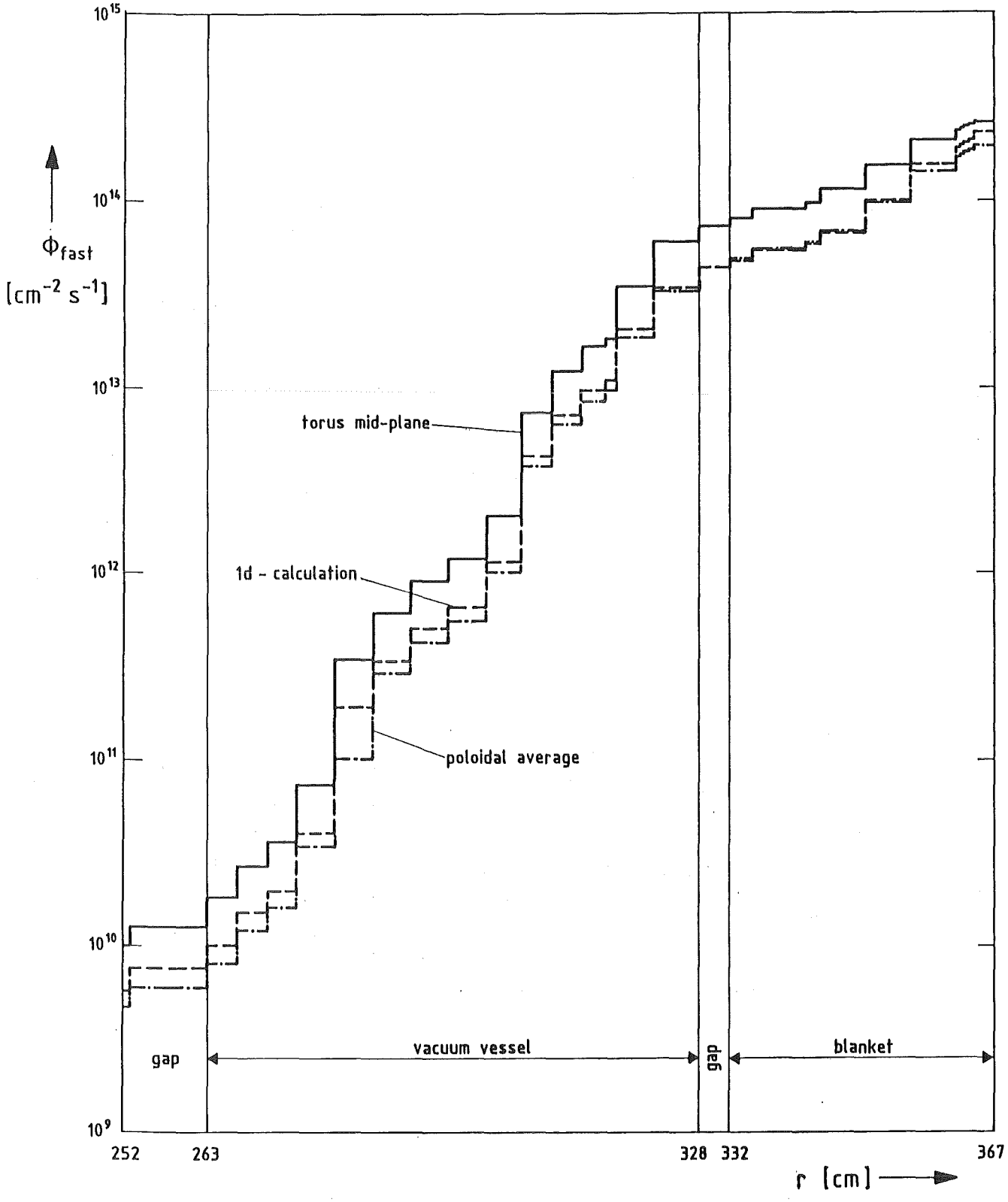

Fig. 12 Radial profile of the fast neutron flux density: poloidal average, peaking value in the torus mid-plane and one-dimensional value.

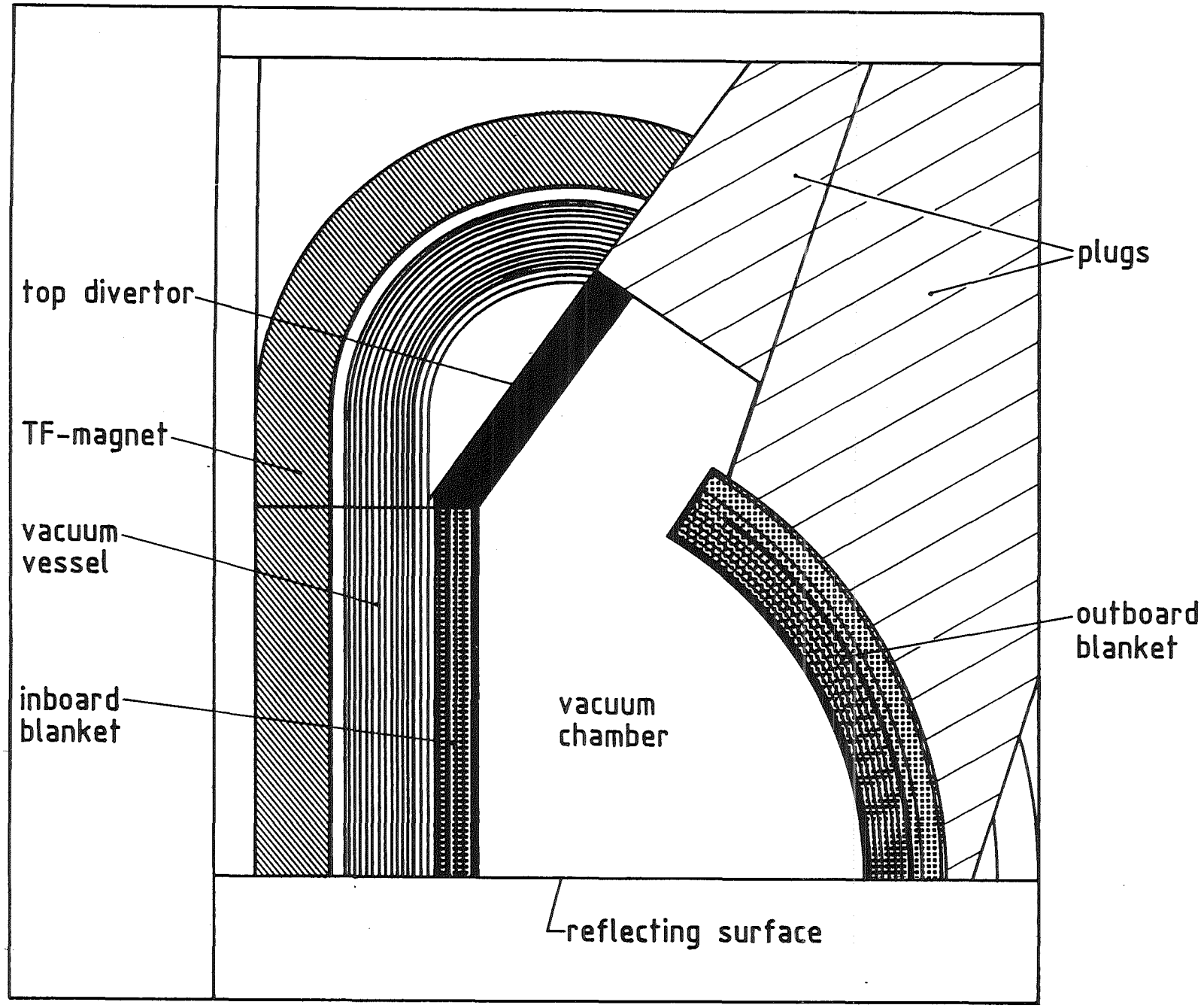

Fig. 13 Radial-poloidal cross-section of the torus sector model used for the divertor shielding calculations.

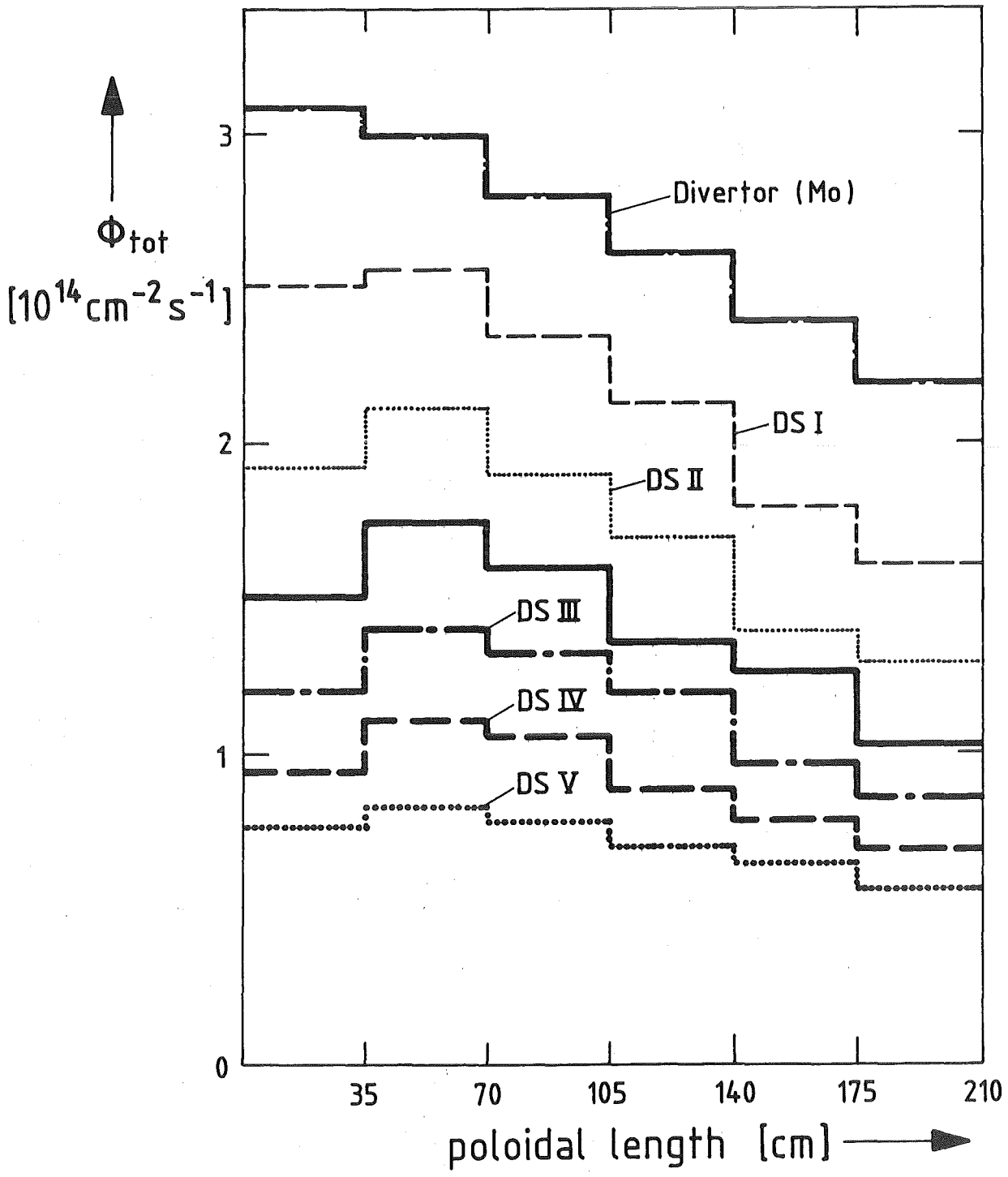

Fig. 14 Poloidal variation of the total neutron flux density in the divertor supporting structure.

DS = Divertor Supporting Structure
(I - IV: Zone division 3 - 35 cm)

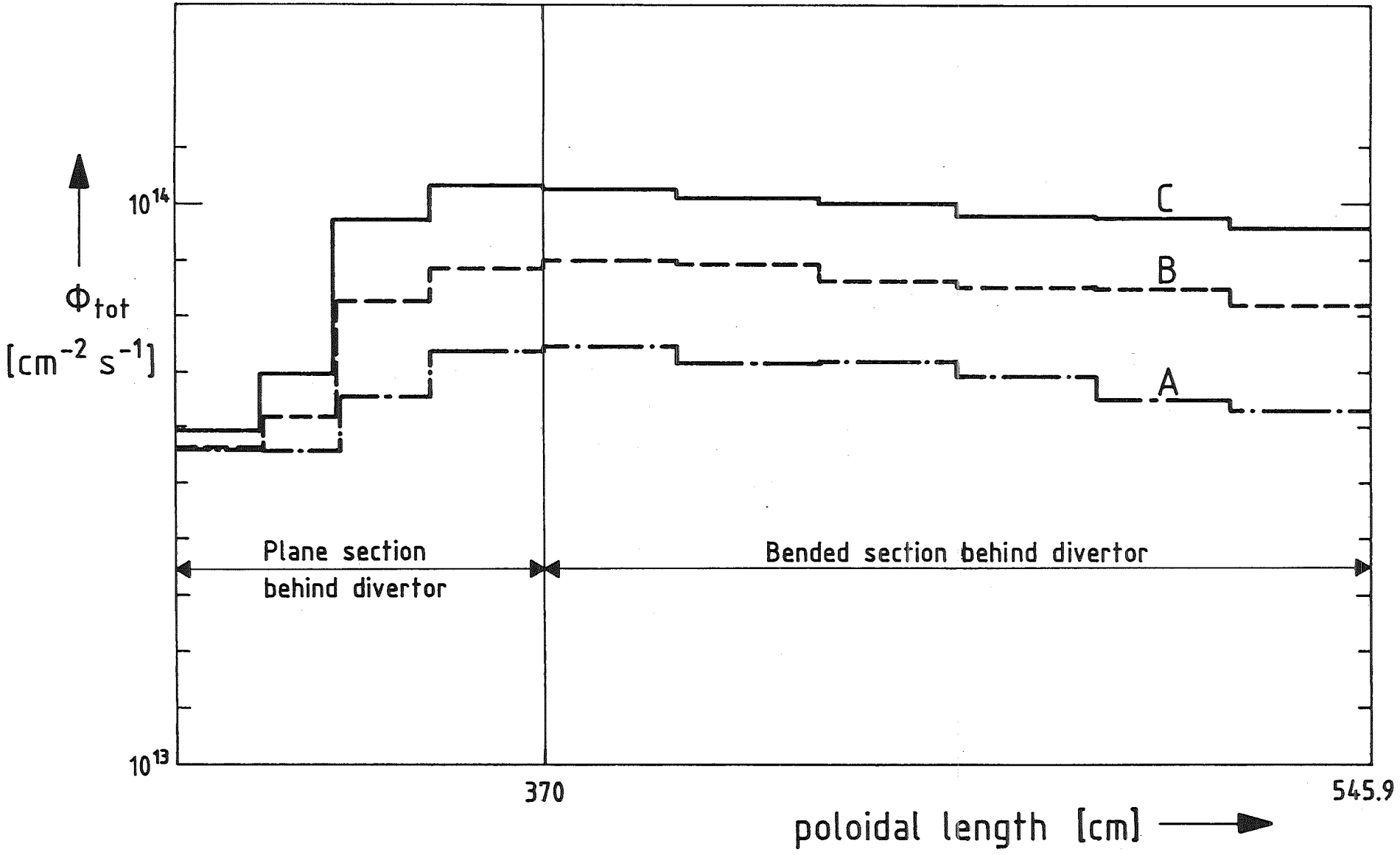

Fig. 15 Poloidal variation of the total neutron flux density at the front of the vacuum vessel in the region behind the divertor.

Effective thickness of the divertor steel supporting structure:
A = 19 cm B = 13 cm C = 7 cm

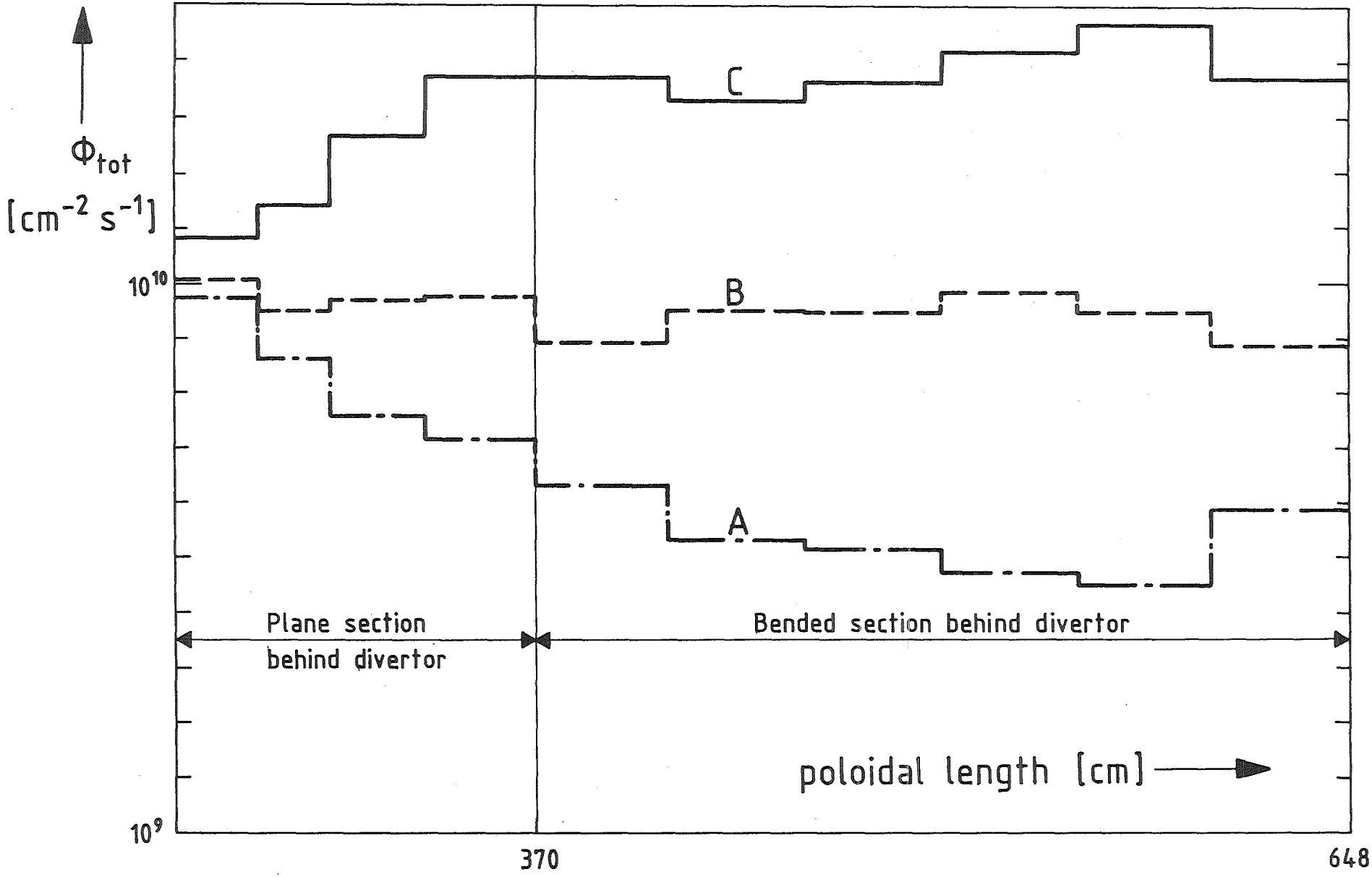

Fig. 16 Poloidal variation of the total neutron flux density at the front of the superconducting magnet in the region behind the divertor.

Effective thickness of the divertor steel supporting structure:
A = 19 cm B = 13 cm C = 7 cm

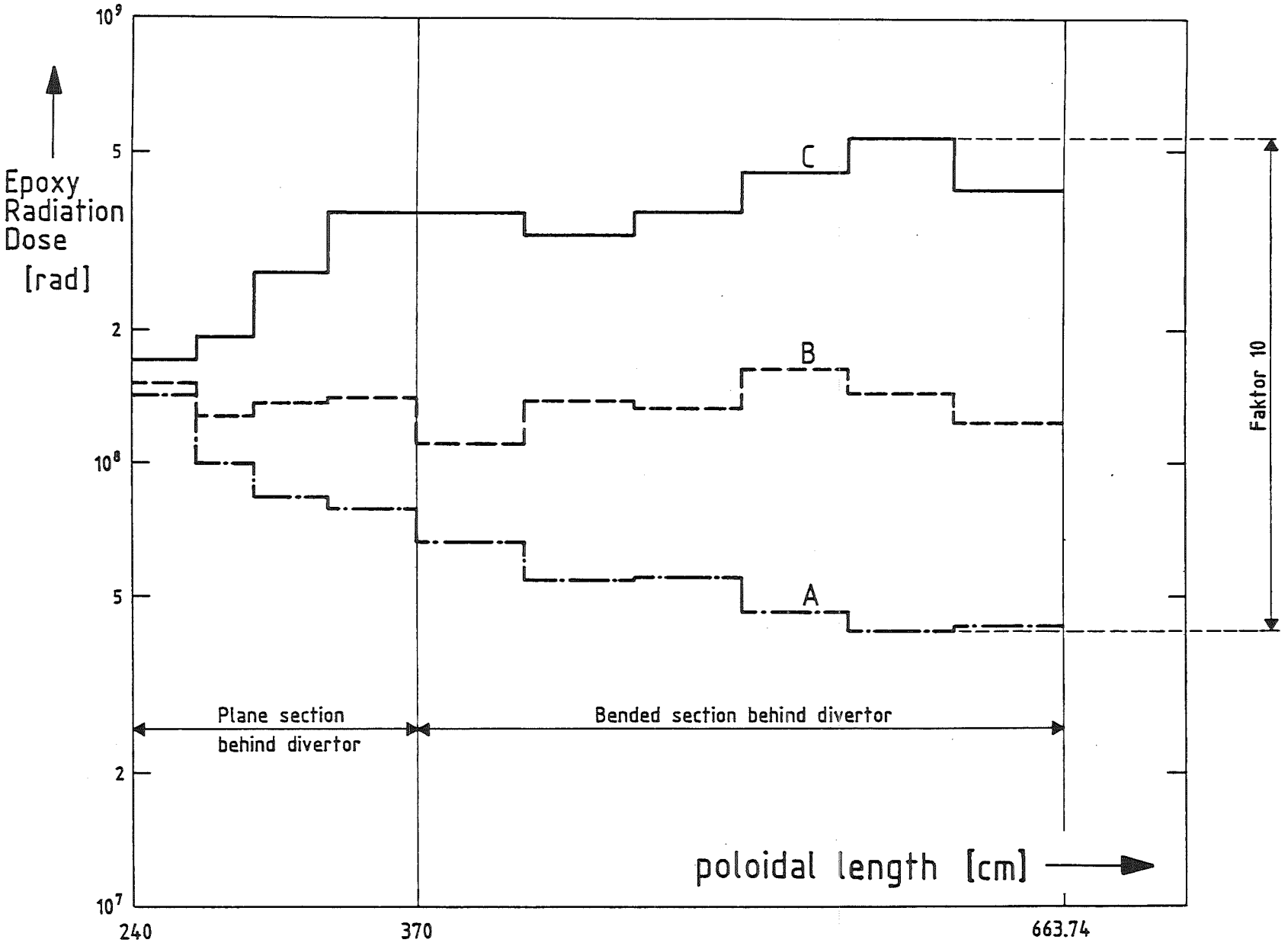

Fig. 17 Poloidal variation of the Epoxy radiation dose in the region behind the divertor.

Effective thickness of the divertor steel supporting structure:
A = 19 cm B = 13 cm C = 7 cm

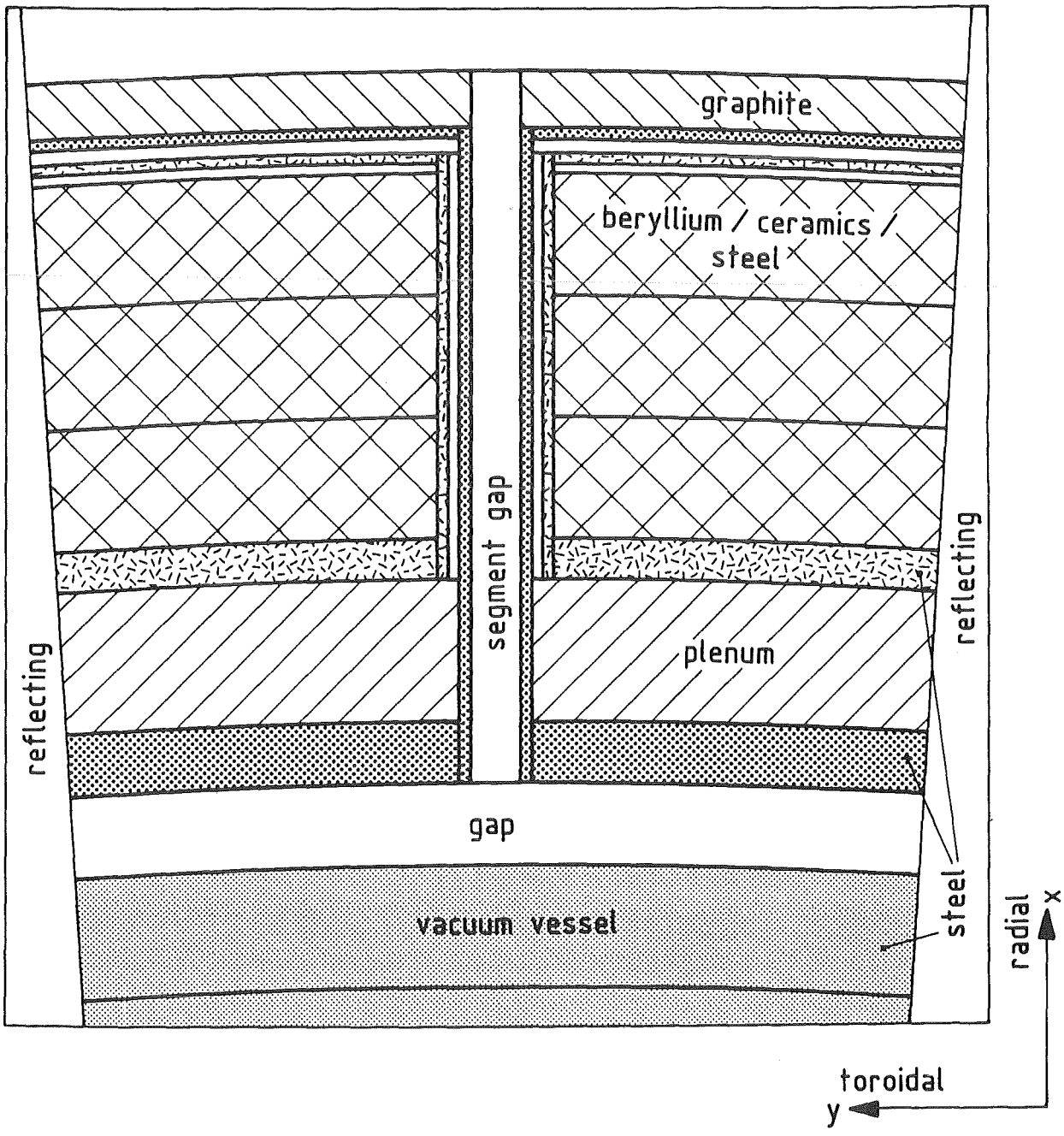

Fig. 18 Two-dimensional sector model for analyzing the neutron streaming through the segment gaps.

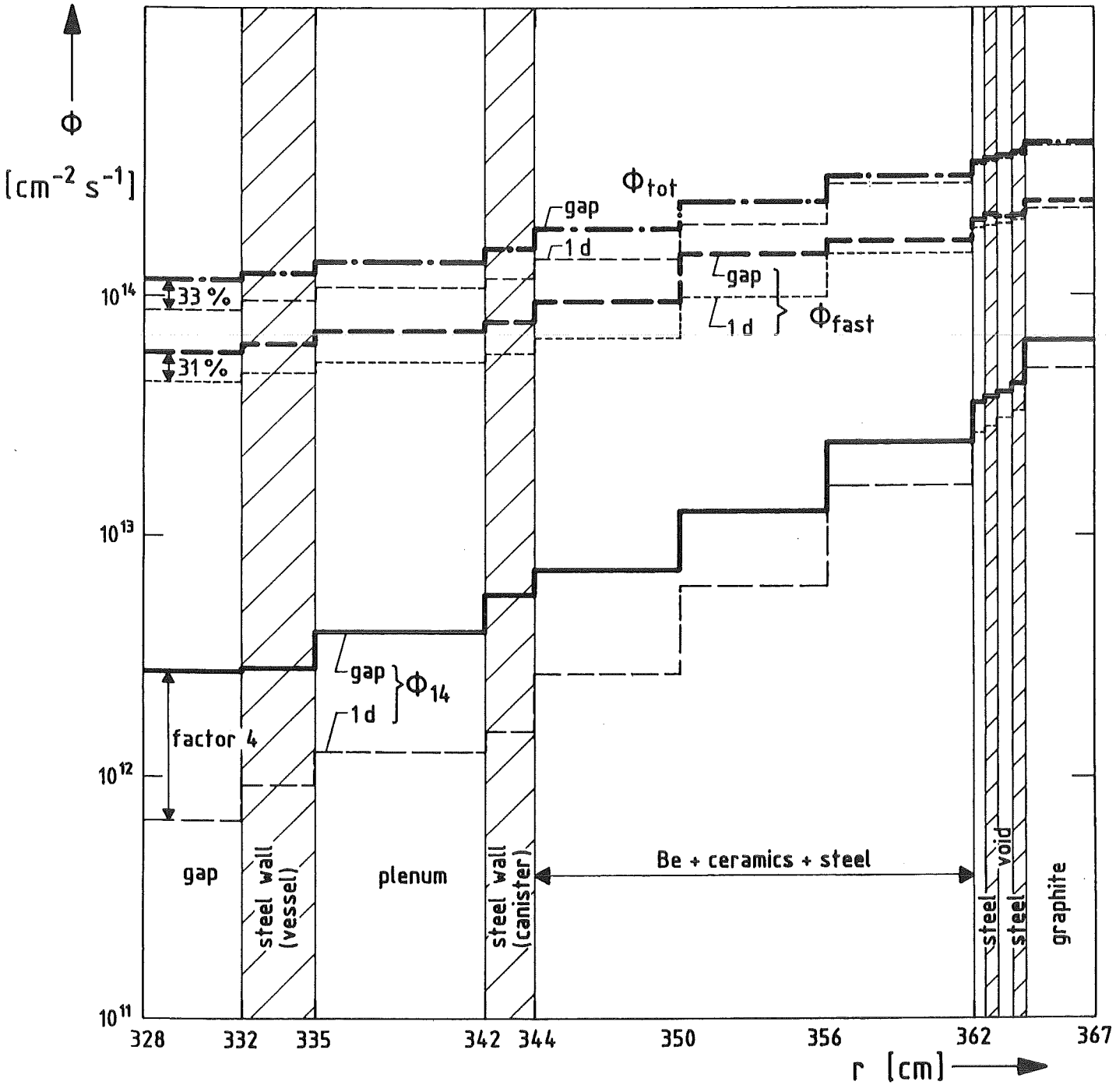

Fig. 19 Radial profiles of the neutron flux densities in the blanket and the segment gap.

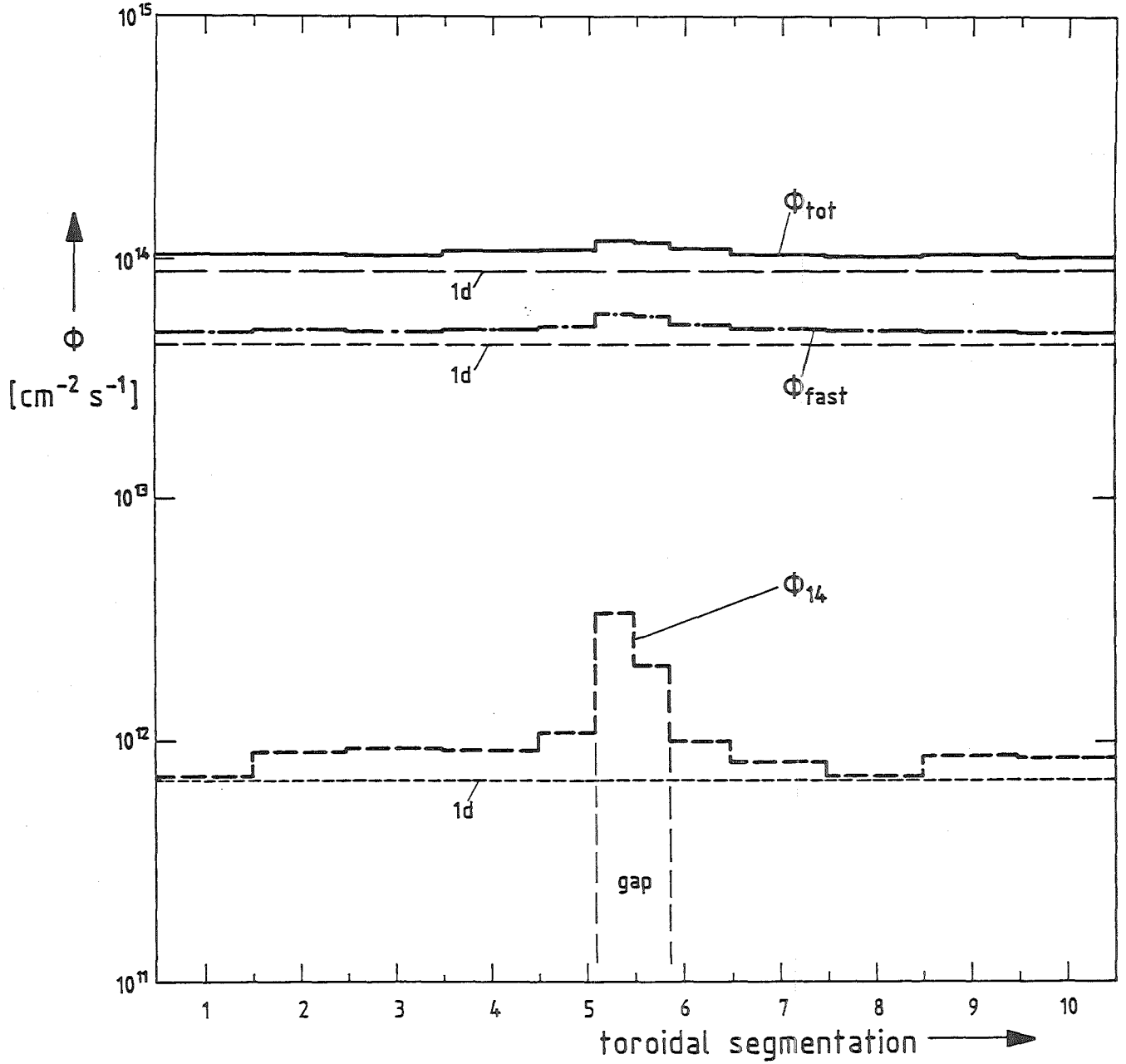

Fig. 20 Toroidal profiles of the neutron flux densities at the front of the vacuum vessel (impact of the segment gap).

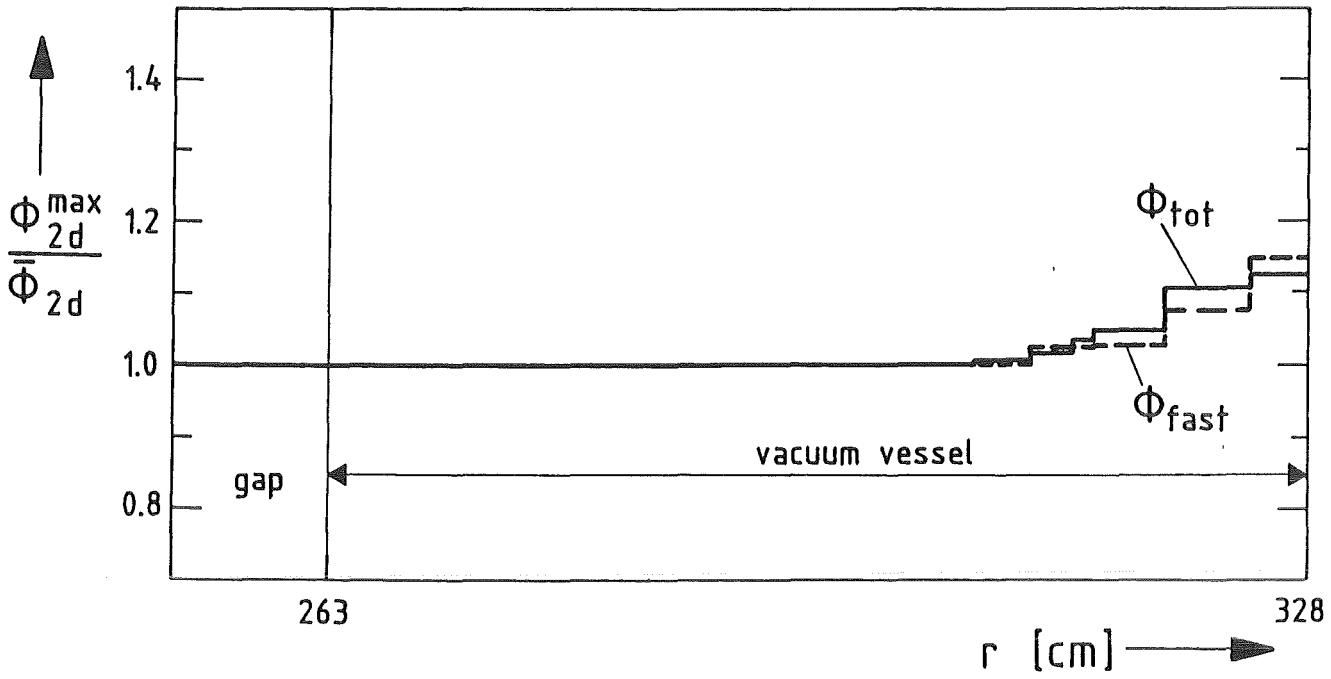

Fig. 21 Toroidal peaking factor of the total neutron flux density in the region of the vacuum vessel (impact of the segment gap).

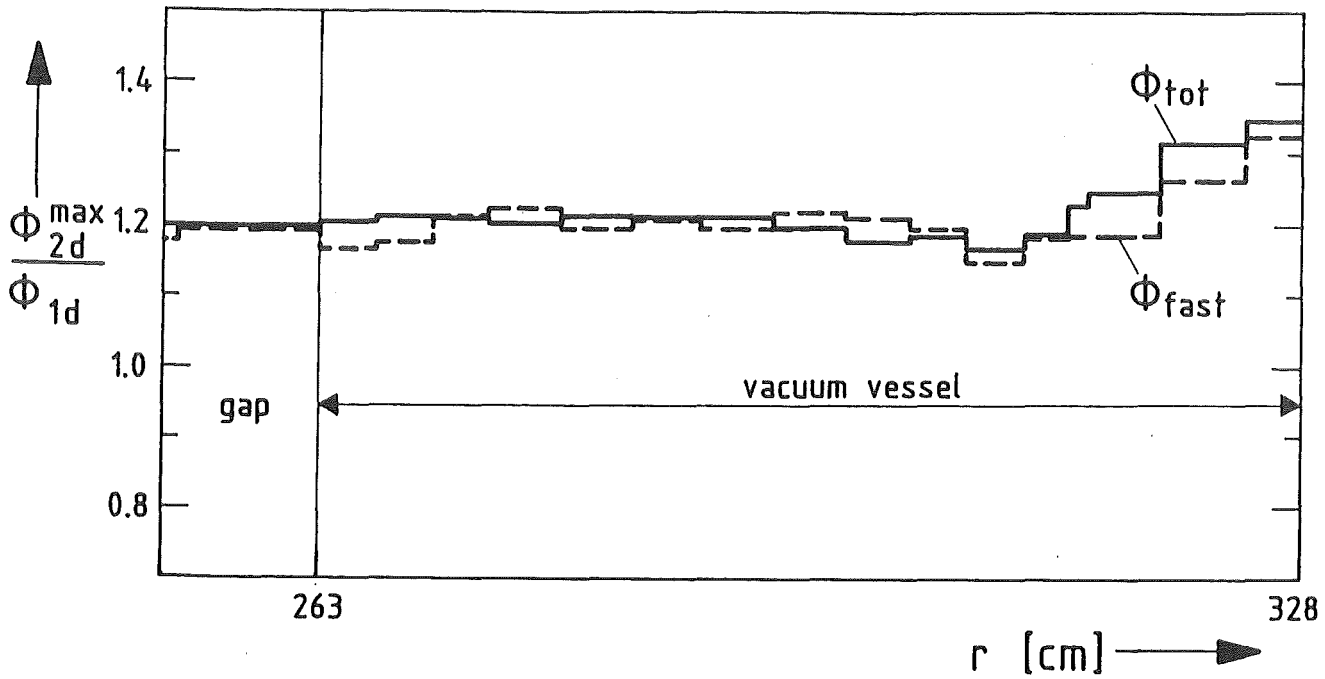

Fig. 22 Impact of the segment gap: ratio of the total neutron flux densities in the region of the vacuum vessel with and without segment gap.